PAC Jeopardy Proposal: Measurement of the Parity Violating Asymmetry in the $N \rightarrow \Delta$ Transition (Originally E97-104)

S.P. Wells (cospokesman), N. Simicevic (cospokesman), K. Johnston, and T.A. Forest
Center for Applied Physics Studies
Louisiana Tech University
Ruston, Louisiana 71272
and
The G0 Collaboration

1 Overview

1.1 Introduction

This proposal has been prepared for the review of the "Parity Violating Asymmetry in the $N \rightarrow \Delta$ Transition" experiment by the Jefferson Lab Program Advisory Committee. This experiment was previously approved as experiment E97-104 with a B^+ priority in February 1997. This proposal has been prepared in accordance with the "jeopardy" rules of Jefferson Lab.

In this experiment, the parity violating asymmetry in inclusive single pion electroproduction from the proton will be measured over a four momentum transfer range of $0.1 \leq Q^2 \leq 0.5$ $(\mathrm{GeV/c})^2$. These measurements will be made with the same equipment as the G0 backward angle measurements are made, and during the same running period as the G0 backward angle measurements, so that no additional resources or beam time are required beyond those allocated for G0 backward angle running. The primary purpose of this experiment is to extract the axial vector transition form factor $G^A_{N\Delta}$ for the $N \rightarrow \Delta$ transition as a function of Q^2, which allows us to extract the axial mass M_A in the Adler parameterization of this form factor. This represents the first determination of this quantity in the neutral current sector of the weak interaction, and in a Q^2 range that is complementary to other experiments (with Q^2 coverage $0.5 \leq Q^2 \leq 2.5$ $(\mathrm{GeV/c})^2$) which use exclusive electroproduction of the Δ^{++} resonance, along with assumptions of PCAC and low energy theorems, to extract this form factor.

Since the time of the original approval of this experiment, significant progress has been made toward the development of the G0 experiment, as will be summarized in this report. Because the measurements proposed here will be performed with the G0 apparatus in its backward angle mode, here we emphasize the developments relevant for backward angle running up to the date of this propsal:

- G0 Management Plan enacted,
- Construction of Superconducting Magnet System (SMS) complete,
- Delivery of SMS to UIUC in progress,

- Construction of liquid hydrogen target complete,
- Design of Focal Plane Detectors (FPD's) complete,
- Fabrication of FPD's in progress,
- Construction of FPD support structure complete,
- Design of Cryostat Exit Detectors (CED's) complete,
- Fabrication of CED's in progress,
- Design of CED support structure in progress,
- Design of CED-FPD coincidence electronics complete,
- Testing of CED-FPD prototype electronics in progress,
- Standard GEANT simulation package developed,
- Background measurements performed in Hall C.

An update of the physics motivation and theoretical work is provided in the next subsection, along with a presentation of our expected results. This is followed by a summary of the experimental configuration to be used. A detailed discussion of the cross section and rate calculations and expected backgrounds is presented in the following sections. For completeness, we include the physics formalism, and a discussion of the nonresonant backgrounds in appendeces.

1.2 Physics Update

This experiment will measure the parity violating asymmetry in single pion electroweak production from the proton, from which the axial transition form factor $G^A_{N\Delta}(Q^2)$ can be determined. This form factor characterizes the axial response of the proton during its excitation to the Δ resonance, and is a necessary ingredient in constraining models of nucleon structure.

Since the original submission of this proposal as PR97-104, there has been a fair amount of theoretical work toward understanding the weak excitation of the Δ resonance. The late N.C. Mukhopadhyay *et al.,* [1] studied in detail the parity violating asymmetry in the $\vec{e}p \to e\Delta^+$ reaction, with particular emphasis on the nonresonant contributions to this asymmetry. They find that the kinematics where these proposed measurements will be made, i.e. relatively low Q^2 and at backward scattering angles, have enhanced sensitivity to $G^A_{N\Delta}(Q^2)$, while at the same time have relatively little contamination from nonresonant contributions. Other authors have investigated the axial transition response in this excitation mode [2], and through neutrino induced Δ^{++} production [3, 4, 5].

Experimentally the measurements proposed here are unique, in that they provide direct access to $G^A_{N\Delta}(Q^2)$ in the neutral current sector of the weak interaction in the low Q^2 regime $0.1 \leq Q^2 \leq 0.5$ (GeV/c)^2. There have been data taken with the CLAS detector in Hall B (E94-005) [6], however, on the $ep \to e\pi^-\Delta^{++}$ reaction in the Q^2 range $0.5 \leq Q^2 \leq 2.5$ (GeV/c)^2, from which $G^A_{N\Delta}(Q^2)$ can be inferred with the assumption of PCAC, and the extrapolation of low energy theorems through the resonance region. These data are still under analysis. While it is true that the measurements proposed here provide direct access to this form factor, there will

generally be contributions from nonresonant terms, even though they have been predicted to be small in our kinematic regime [1]. Understanding these nonresonant pieces has also been the subject of recent work [7], where it is demonstrated that these terms can be extracted through polarization observables in the $p(\vec{e}, e'\vec{p})\pi^0$ reaction. Additionally, the inclusion of nonresonant terms proved to be important in a model which was used to describe recent $(e, e'\pi^0)$ data from both Jefferson Lab and MIT-Bates [8]. The physics program in Hall B at Jefferson Lab includes polarization observables in single pion electroproduction reactions, from which a determination of these nonresonant terms will be made at the 5% level [9], which will be sufficient to constrain these contributions to the $N \rightarrow \Delta$ asymmetry measurement at the level required to extract $G^A_{N\Delta}$.

It is worth mentioning at this point that the proposed measurements will provide a characterization of the axial response of the proton during its transition to its first excited state, the Δ resonance, while the recent results from the SAMPLE experiment [10] at MIT-Bates on the parity violating asymmetry in quasielastic electron scattering from deuterium suggest that the axial response in *elastic* electron proton scattering is not understood. These issues will be addressed by the G0 backward angle quasielastic measurements on deuterium, for which a letter of intent will be submitted to this PAC, and beam time request made at the next PAC. Because the expected beam time for backward angle G0 measurements will be split between measurements from the proton and measurements from deuterium, only 1/2 of the beam energies originally expected will be used for the $N \rightarrow \Delta$ measurements from the proton. Consequently, not as large a Q^2 range will be covered as originally expected. Nonetheless, when the measurements proposed here are taken into account along with the quasielastic measurements from deuterium, a more coherent picture of the axial response of the proton in general will likely emerge.

Shown in Fig.'s 1 and 2 are the expected results for these measurements. In Fig. 1, expected results for the parity violating asymmetry in single pion electroweak production from the proton are plotted, along with a model [11] which breaks the contributions to this asymmetry into its resonant and nonresonant parts. In Fig. 2, we plot the expected results for extraction of the axial transition form factor $G^A_{N\Delta}$ as a function of Q^2. Although our determination of this form factor is in the neutral current sector of the weak interaction, while the neutrino induced results are in the charged current sector, so that a direct comparison cannot truly be made, we show on this plot the allowed range of shapes of this form factor in the Adler parameterization [12] using the uncertainties on the extracted axial mass M_A from the neutrino results. With the expected statistical precision for the proposed measurements, we expect an uncertainty on the axial mass of $\delta M_A \sim 0.045$, roughly a factor of two better than the best constraints from the neutrino experiments.

1.3 Equipment Udpate

As discussed in the introduction, there has been significant progress in the development of the equipment required for the G0 experiment. In this section, we present a brief summary of this progress, with particular emphasis on those subsystems required for backward angle running.

1.3.1 Superconducting Magnet System

At the heart of the G0 experiment is a superconducting magnet system (SMS), consisting of a toroidal array of eight superconducting coils with a maximum field integral of approximately 1.6 T·m. The spectrometer is designed to focus particles of the same momentum and scattering angle

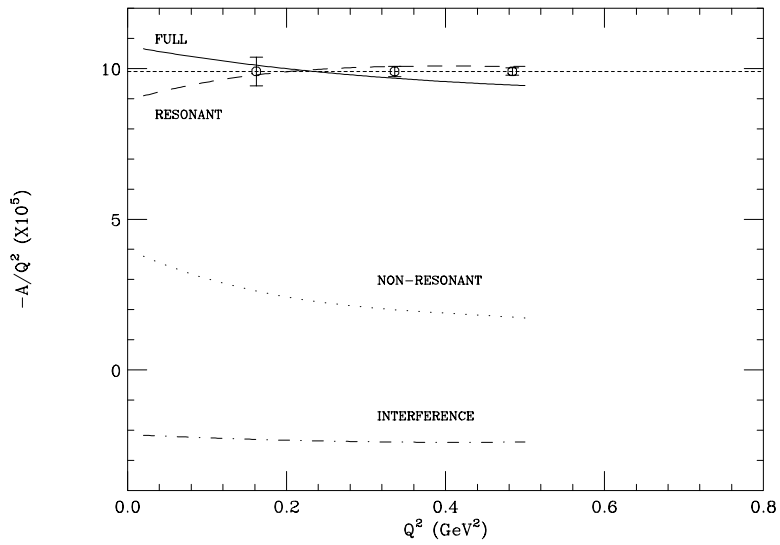

Figure 1: Expected asymmetries for the $\vec{e} + p$ inelastic reaction at the peak of the Δ resonance. The result of the full calculation [11] (solid line) is compared to the contributions of the non-resonant background (dotted line), resonance (long dashed line), resonance neglecting the contribution from the axial form factor $G^A_{N\Delta}(Q^2)$ (short dashed line), and interference term (dot-dashed line). Included are the expected statistical uncertainties of our measurements in the several Q^2 bins of the reaction to be measured.

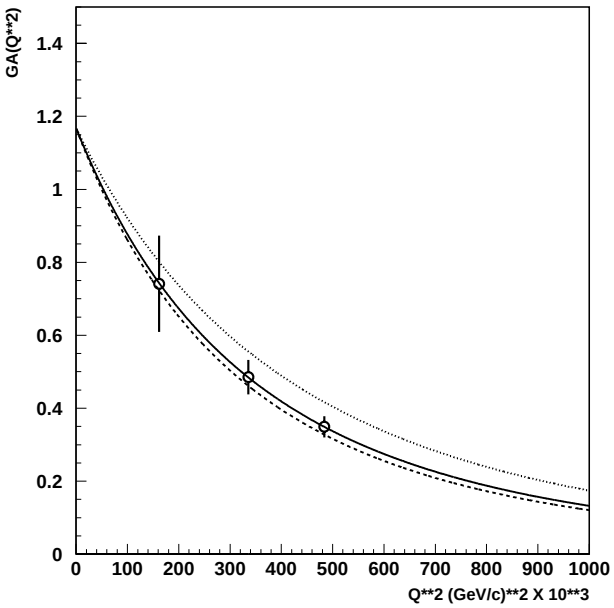

Figure 2: Axial vector transition form factor $G^A_{N\Delta}$ plotted vs. Q^2 assuming the Adler parameterization. Errors represent expected statistical errors only, and the allowed kinematical region for electrons from 2-π production has been excluded. The dotted and dashed lines above and below the solid line represent the limits on the shape of this form factor from the uncertainty on the axial mass M_A from neutrino experiments ($\delta M_A = 0.09$). From the results expected here, we will achieve $\delta M_A = 0.045$.

from the length of an extended target to a single point, i.e. zero magnification in the dispersion direction [13]. At backward angles, elastically scattered electrons can be efficiently measured using beam energies up to 2.2 GeV. The overall acceptance of the spectrometer is defined by lead collimator modules positioned inside the cryostat, and for elastically scattered electrons in this configuration, is 0.5–0.9 sr.

The SMS toroid was contracted out to BWX Technologies, who included the collimators and assembly fixtures into the magnet. The entire assebly has been completed, and a photograph of the spectrometer during its assembly is shown in Fig. 3, in which the superconducting coils, many of the lead collimators, and cryoplumbing are shown. The performance of the magnet design has been checked optically at BWX, through a procedure which measured the locations of the coils and collimator modules within the cryostat at 80 K, where most of the thermal contraction has already taken place. The spectrometer has been delivered to UIUC, where magnetic verification will be performed through the Spring of 2001, after which time the SMS will be delivered to Jefferson Lab.

A separate controls system including interlocks, signals, instrumentation, and quench protection circuitry has also been developed to ensure safe operation of the magnet.

1.3.2 Cryogenic Target

Significant progress on the construction of the cryogenic loop and its associated hardware has been made since the original submission of this proposal. All parts of the loop have been machined, the loop assembled, including all instrumentation, and the gas handling system for the hydrogen and helium cells has been constructed. The target service module, which is a vacuum vessel positioned on the beamline directly upstream of the target and supports the loop, includes the transverse motion mechanism and gas and electrical service lines to the loop, has been designed with appropriate specifications. A quote for this hardware has been provided by Thermionics Northwest, and construction will commence following the completion of a contract between Jefferson Lab and Thermionics.

The controls/ monitoring/ interlock hardware has been completely specified, with all commercial products purchased, and most of the custom electronics completed. The EPICS based controls software for the target has been specified, with the JLab Accelerator Division software support group overseeing its completion.

In order to perform thorough testing of the target at cryogenic temperatures before its installation into the G0 spectrometer, space in the EEL for a test bench, and time for use of cryogenic services in this building have been allocated to the G0 target group. The target loop will be delivered to JLab in the upcoming spring, with testing commencing through the spring and summer before installation into Hall C next winter.

1.3.3 Detectors

The detector system to be used for these backward angle measurements consists of two arrays of scintillators for each of the eight G0 octants: a Focal Plane Detector (FPD) array (sixteen detectors per octant each viewed from two ends), which will also be used for the forward angle measurements, and a Cryostat Exit Detector (CED) array (nine detectors per octant each viewed from two ends). For backward angle electron detection, both arrays are required to determine the electron scattering angle and momentum, thereby providing an adequate separation between

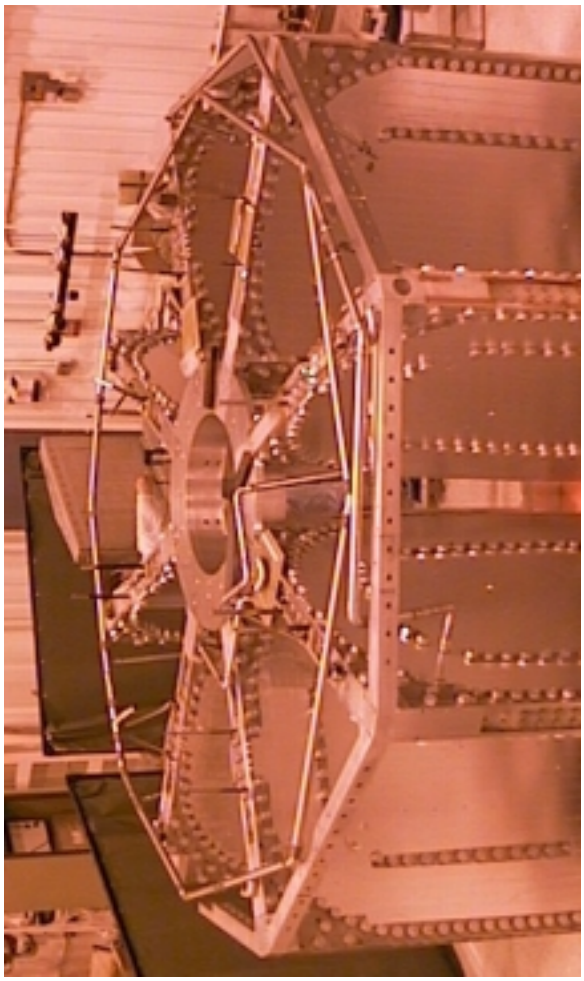

Figure 3: Photograph of SMS assembly at BWXT.

elastically and inelastically scattered electrons.

The FPD's are being constructed in two sets of four octants: one set by a North American component of the collaboration, and one set by the French component. The North American effort is nearly complete. All scintillators and most of the light guides for all four octants have been delivered to JLab, the octant mechanical supports and "ferris wheel" have been constructed and are in house at JLab, all photomultiplier tubes and base assemblies are in house at JLab, and the detector assembly (gluing, wrapping, and mounting into the octant supports) is nearly complete. Shown in Fig. 4 is a photograph taken during the assembly of one octant of detectors, where the first four of sixteen scintillator/light guide/PMT assemblies have been installed into the octant support. Shown in Fig. 5 is a photograph of the "ferris wheel" support structure, which supports each of the individual octant supports, with one octant support installed as a test of the fit of the supports into the "ferris wheel" and as a demonstration of the installation procedure.

Significant progress has also been made for the French FPD octants. The design of the scintillators and light guides are complete, and the construction has been contracted out to a vendor. The design of the octant support structures has also been completed and contracted out. Procedures have also been established for safe transportation to JLab, and for survey and final assembly at JLab. The PMT/base assemblies to be used for the French detectors is somewhat different then those to be used for the North American ones, in that the French bases include a times ten amplifier utilizing Zener diodes (related to radiation concerns), and final tests of prototype bases have been completed. All PMT's have been ordered, delivered, and tested. The French effort is presently on schedule to deliver the last of four octants to JLab by June 2001.

There is presently a plan to position one full octant, complete with detectors, PMT/base assemblies, and full cabling into Hall C during the $\vec{d}(\vec{e},e'n)p$ G_e^N experiment scheduled to be run starting in July 2001. This effort will serve the dual purpose of testing a fully integrated octant of detector/cabling/electronics/data acquisition for forward angle measurements, and providing some measure of room background expected during the G0 measurements.

The CED's are a critical component of the G0 backward angle running, and here we provide a summary of the progress to date on this detector package. In the original proposal, there were to be twelve individual CED's per octant, to be combined with the sixteen FPD's. Due to space constraints between the magnet end cap, beam line shielding, and the FPD octant support, three of the CED's closest to the beam line were eliminated from the design, leaving nine CED's per octant. Because these three CED's which were removed intercepted a large yield of lower momentum inelastically scattered electrons, our momentum transfer range does not reach as low as originally proposed, and our statistical uncertainty at lower momentum transfer is somewhat larger than originally expected (as can be seen in Fig.'s 1 and 2). In addition, the lower momentum inelastically scattered electrons at each beam energy are no longer included, resulting in fewer Q^2 bins for the asymmetry measurement and axial transition form factor extraction.

The design of the remaining nine CED's has been completed, including the shapes of both the scintillators and light guides, and a procedure for manufacturing the correct shapes for the light guides has been developed and tested in the construction of a prototype CED. A detailed simulation of expected light yield from these detectors was performed, and the number of photoelectrons predicted was found to be more than adequate for these measurements. A prototype CED was constructed at TRIUMF, and tested at Louisiana Tech University using the same PMT/base assemblies to be used in the North American FPD's, and the amount of light collected was

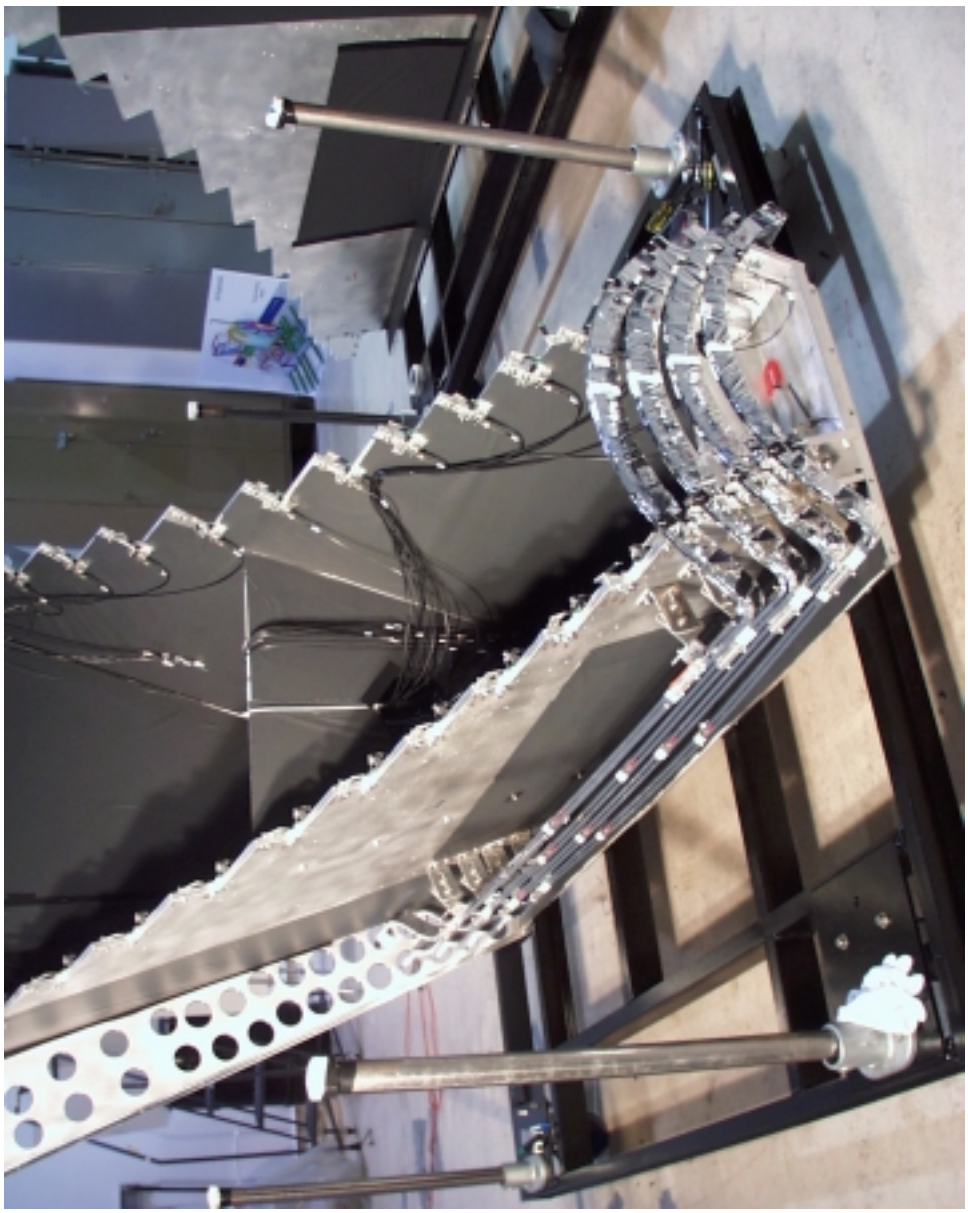

Figure 4: Photograph of FPD's 1 through 4 mounted into the FPD octant support during assembly.

Figure 5: Photograph of "ferris wheel", with one octant support installed, along with one collaborator to set the size scale.

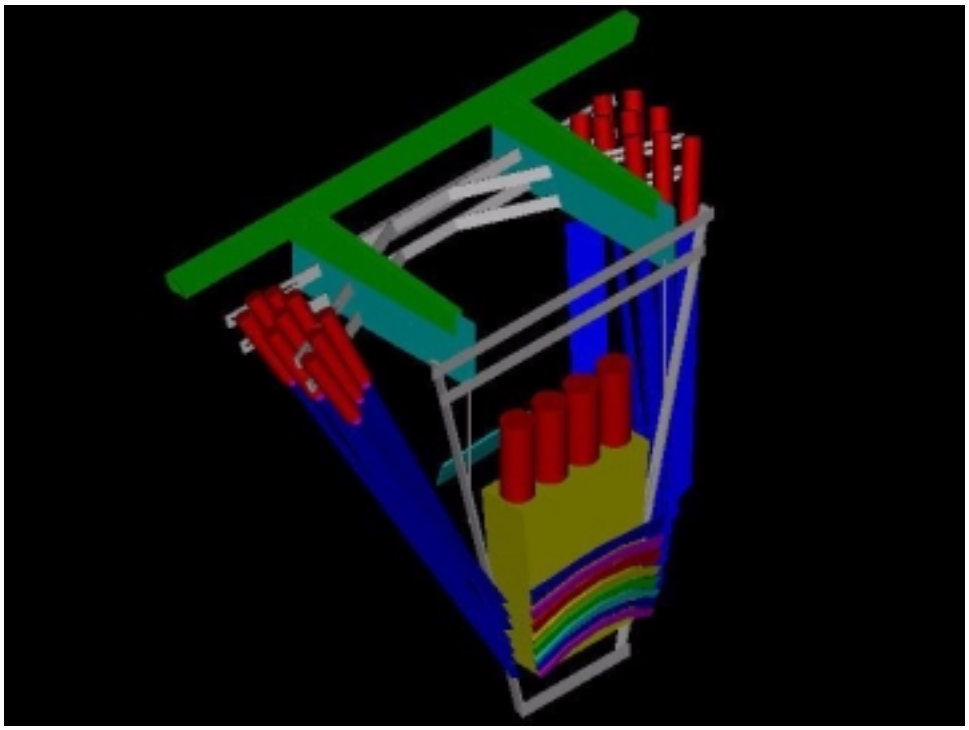

Figure 6: Schematic diagram of the CED octant support structure, showing the relative locations of the scintillators, light guides, and PMT's. Also shown is a possible position of a Čerenkov detector for G0 backward angle deuterium measurements.

consistent with the predicted amount, i.e. more than adequate for these measurements [14, 15].

The construction of the CED's has just begun in the TRUIMF scintillator shop. All of the scintillator material has been purchased and shipped to TRIUMF, and approximately one half of the light guide material is on hand. The present schedule calls for delivering the cut and polished scintillators and light guides to JLab in the Summer 2001, when assembly of the detectors will begin.

The design of the octant support structure for the CED's is presently underway. The conceptual design, a schematic of which is shown in Fig. 6, is complete, and takes into account both the required mechanical support of the CED scintillator/light guide/PMT and base assemblies, as well as the relatively weak alignment constraints on these detectors. Also shown in this figure is the relative positions and shapes of the CED's, light guides, and PMT's. Each octant support will be attached to the outer ring of the "ferris wheel" to provide the main mechanical support, in the region of the CED assembly near the PMT's where the majority of the weight of these detectors resides. The positioning of the scintillators, as well as additional mechanical support, is obtained through the use of cantelevered struts extending from the main support through the region near the bend in the light guides outside of the acceptance of the scattered electrons.

1.3.4 Backward Angle Electronics

As discussed in the original proposal for these measurements, much of the electronics used for the forward angle G0 measurements will be used for the backward angle running, and only a small part of the electronics will be different. Since that time, the decision has been made for the forward angle measurements to instrument the French FPD octants with the IPN-Orsay electronics design (DMCH-16X board) based on flash-TDC and DSP technology, while the North American octants will be instrumented with the original Latching Time Digitizer (LTD) design. Nonetheless, for both cases, much of the electronics used for forward angle measurements will be used for the backward angle running. In particular, all of the PMT/base assemblies and associated power supplies used for the backing scintillator array for the FPD's will be used for the CED's, and all of the instrumentation for the backing array (e.g., analog splitters, constant fraction discriminators, mean timers, and ADC and TDC channels for the monitoring electronics) is also available for the CED array.

The North American electronics chain for forward angle measurements is shown schematically in Fig. 7. For the backward angle measurements, the PMT's for the FPD backing detector array will be attached to the CED's, and the LTD's and "munger" redistribution boards will be replaced by custom logic circuitry being developed at Louisiana Tech. Thus, the input to this new logic circuitry is the output of the mean timers for both the FPD's and CED's, along with a synchronization pulse which signals the arrival of the beam at the G0 target, and the output is sent to the latching scalers to count the number of coincidences between detectors in the CED array and those in the FPD array.

Significant development on the coincidence logic circuitry for the North American octants has taken place since the time of the original proposal. The circuit design, which is now complete, involves the use of Programmable Logic Devices (PLD's), in which all of the logic associated with the CED-FPD coincidences, handling of "multiple hit" events (where more than one CED or more than one FPD fires on a given beam burst) and dead time monitoring is contained. Enough of the PLD's have been obtained to construct all necessary prototype circuit boards, the programming software to burn these chips has been obtained, debugged, tested, and used for programming, and properties of the programmed PLD's as well as the logic contained in the programs have been tested. The board layout for the prototypes is complete, and these boards have been manufactured by a vendor. Stuffing and testing of these prototypes is now underway. In the final configuration, a total of five boards will be needed per octant: one to handle the coincidence logic encoding, one to handle the multiple hits, and three to handle TTL-ECL conversion to provide the appropriate level required by the latching scalers. All of the boards will be housed in a custom VME chassis which provides the necessary power and common ground to each.

The philosophy of the backward angle electronics design is based in large part on the fact that it is the electrons which are detected. In the momentum range of electrons accepted (≥ 200 MeV), these relativistic electrons are all moving with approximately the same velocity, and therefore have a well defined flight time for each CED and each FPD. This is shown in Fig.'s 8 and 9, where we plot the flight time from the target to selected CED's and FPD's, respectively. Thus, a relatively tight time correlation can be made between a given CED and FPD pair and the arrival time of the beam at the LH_2 target. Consequently, fast logic devices, such as the PLD's on hand, can provide hardware coincidences which can significantly reduce time uncorrelated as well as some target related backgrounds. We will return to this point during the discussion of

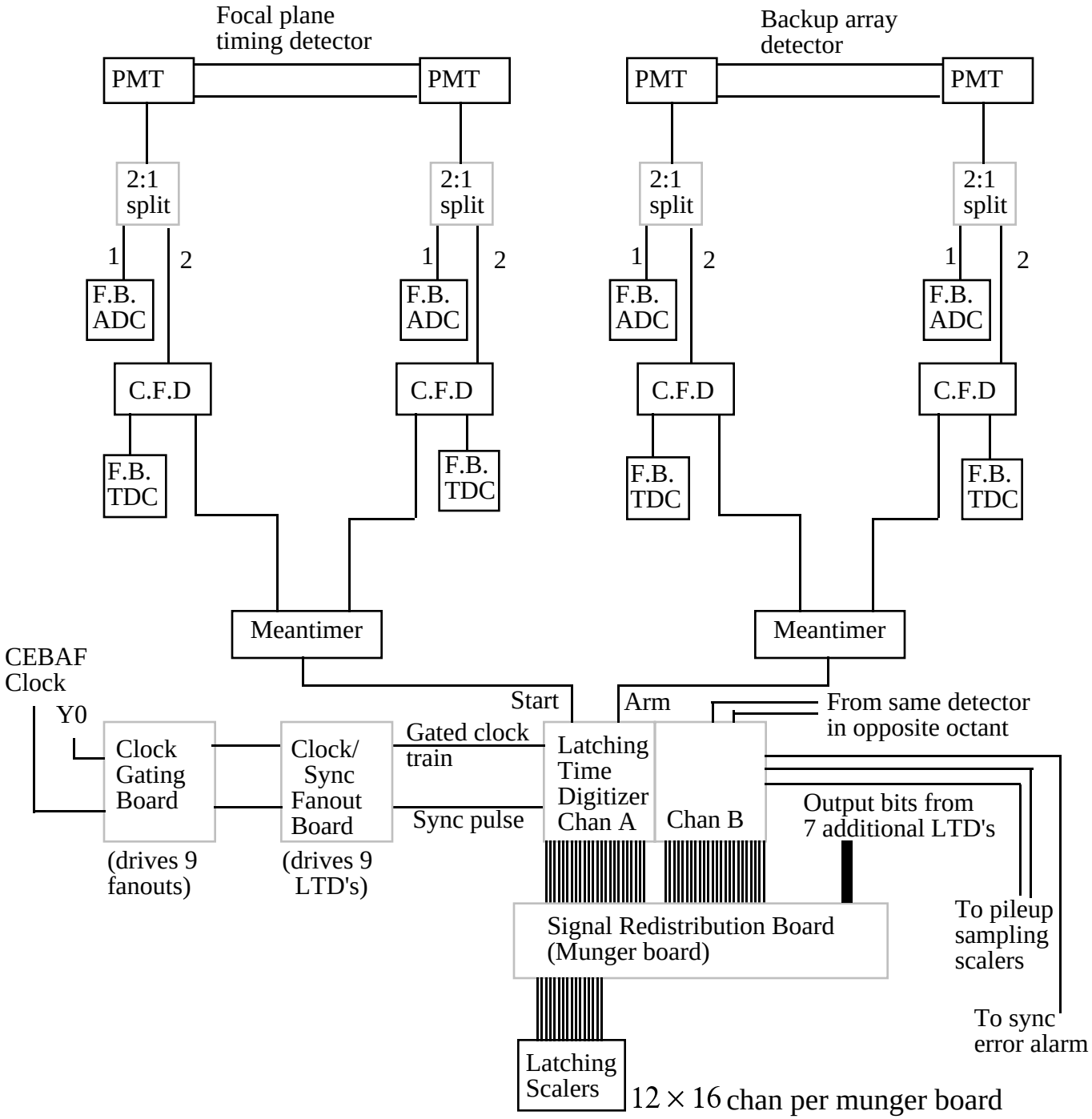

Figure 7: Electronics block diagram for the forward angle running mode for the North American octants.

background considerations later.

Nearly identical logic and overall philosophy for the backward angle measurements will be utilized in the French octants. In this case, however, the front end instrumentation (splitting, discrimination, and mean timing) will be handled by the DMCH-16X boards, and the logic for CED-FPD coincidences, multiple hits, and dead time monitoring will be performed on a separate board which interacts with the DMCH-16X boards through the VXI backplane. Because the DMCH-16X boards also have the capability of acquiring time of flight information, some fraction of the CED-FPD coincidences will also have TOF spectra accumulated in this scheme.

1.3.5 Simulation

A standard GEANT simulation package has been developed for the G0 experiment, which includes the correct shapes for the magnet, collimators, and detectors. This simulation package has been used to estimate our acceptance and rates for these measurements, which we describe in the following sections, and for a detailed estimation of target related backgrounds, which we discuss in a later section.

2 Kinematics and Cross Section Calculation

The design of the $N \rightarrow \Delta$ transition experiment in this proposal has several constraints which have already been taken into account. The G0 spectrometer and associated collimator design is optimized for elastic forward proton and backward electron scattering, and can be used for the $N \rightarrow \Delta$ transition asymmetry measurements with no modification. For these inelastic asymmetry measurements made during the same running period that the elastic electron-proton asymmetry measurements are made, we can not alter any of the G0 spectrometer settings.

The asymmetry in the $N \rightarrow \Delta$ channel will be measured with the G0 spectrometer in the backward angle measurement mode. In this configuration, elastically scattered electrons are detected in an angular range centered around $\theta_e \sim 110^\circ$. Using the magnetic field setting, target position and target length for the elastic channel settings, we can calculate the kinematical limits for the inelastic electrons, which are shown in Table 1.

The measurement of the $N \rightarrow \Delta$ asymmetry using the G0 spectrometer is an inclusive measurement, in which only inelastically scattered electrons are detected. The calculation of the cross section in this kinematical range is based partially on the work of J. W. Lightbody and J.S. O'Connell [16] and F.W. Brasse *et al.* [17, 18]. The inelastic electron scattering cross section is calculated as the product of the virtual photon flux and the total cross section for virtual photon-proton scattering, as a function of Q^2 of the virtual photon and the invariant mass of the photon-proton system. The calculation of the total cross section for virtual photon-proton scattering is based on the parametrization by Brasse *et al.* [17, 18]. The results for some electron angles are shown in Fig. 10 for an electron beam momentum of E=0.585 GeV.

The calculation of the Δ electroproduction cross section for the beam energies below 1 GeV is in good agreement with the existing data [16], and can be used to estimate the rates and uncertainties for the $N \rightarrow \Delta$ asymmetry measurements.

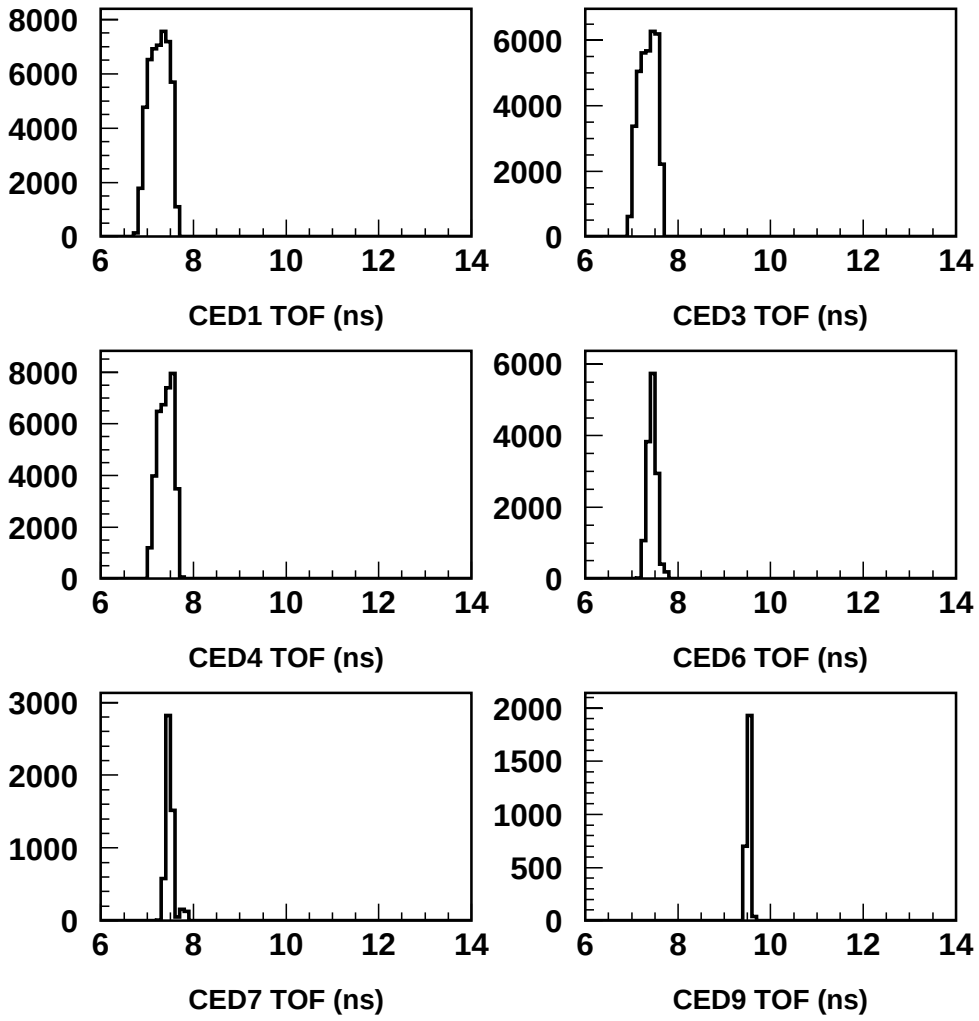

Figure 8: Flight times for electrons from the target to selected CED's.

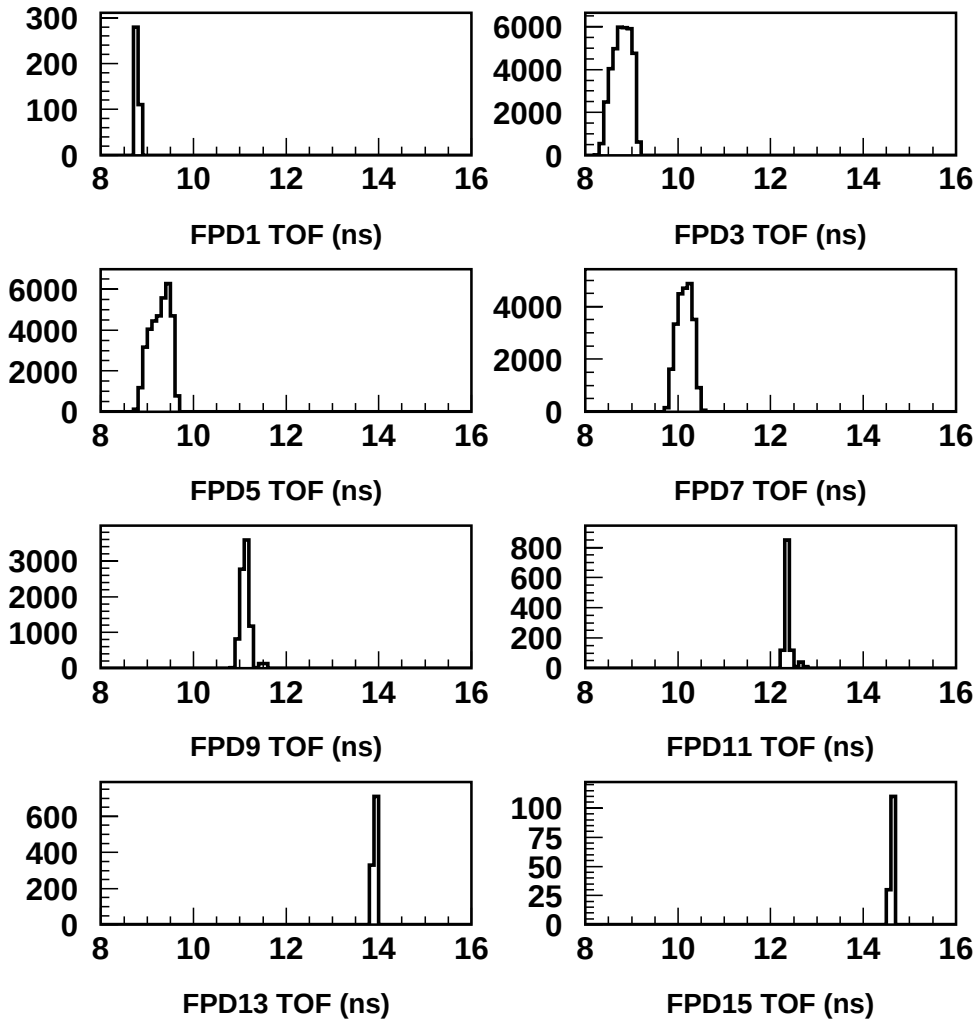

Figure 9: Flight times for electrons from the target to selected FPD's.

$E(GeV)$	$Q^2_{el.}((GeV/c)^2)$	$Q^2_{inel.}((GeV/c)^2)$	$E'_{inel.}$ (GeV)	$\theta'_{inel.}(deg)$
0.424	0.3	0.04 - 0.22	0.060 - 0.190	90 - 105
0.585	0.5	0.10 - 0.40	0.070 - 0.270	90 - 110
0.730	0.7	0.10 - 0.58	0.070 - 0.320	90 - 111

Table 1: Inelastic kinematics for magnetic fields optimized for the elastic channel, calculated for three beam energies.

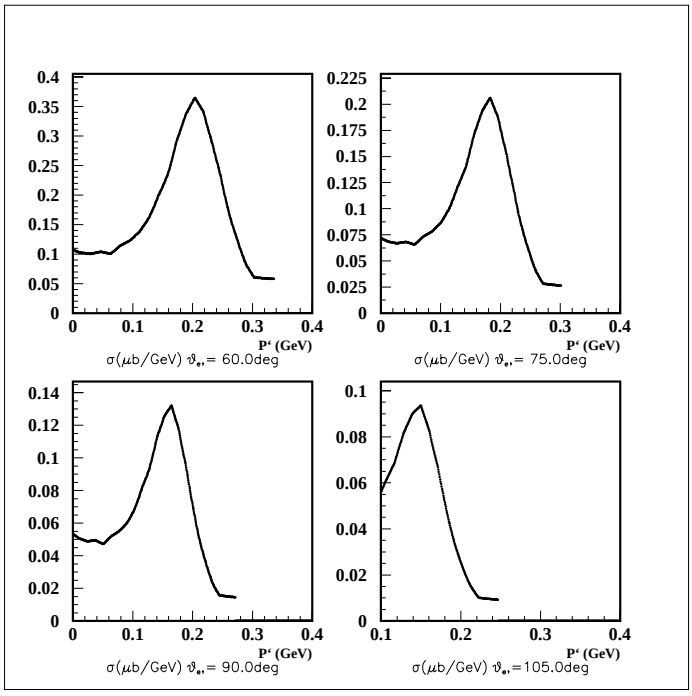

Figure 10: Inelastic electron-proton cross section calculations for E=0.585 GeV, at four electron scattering angles.

3 Rates

The rates for the inelastically scattered electrons are calculated as:

$$Rates = \int_{E'_{min}}^{E'_{max}} \int_{\Delta\Omega} \frac{d\sigma}{dE' d\Omega} dE' d\Omega \tag{1}$$

where $\frac{d\sigma}{dE' d\Omega}$ is the double differential inelastic electron cross section, E'_{min} and E'_{max} are the lower and upper limits of the detected electron momentum, and $\Delta\Omega$ is the covered solid angle. For the inelastic channel, the scattered electron momentum range $\Delta E'$ and solid angle $\Delta\Omega$ are small enough in each Focal Plane Detector-Cryostat Exit Detector coincidence measurement to allow Eq.(8) to be replaced by:

$$Rates = \overline{\frac{d\sigma}{dE' d\Omega}}\ \Delta E'\ \Delta\Omega, \tag{2}$$

where $\overline{\frac{d\sigma}{dE' d\Omega}}$ is the average inelastic electron cross section for electrons having a momentum range $\Delta E'$ detected in the solid angle $\Delta\Omega$.

The measurement of the $N \rightarrow \Delta$ channel in these measurements is broken into many of $\Delta\Omega$ and $\Delta E'$ bins, depending on the number of Focal Plane Detectors and Cryostat Exit Detectors used in the experiment. The analysis of rates is done by assuming coincidences between 9 Cryostat Exit Detectors and 16 Focal Plane Detectors. The total number of possible FPD-CED coincidence combinations is 144, but due to the allowed phase space for single pion production, only a portion of these are used for the $N \rightarrow \Delta$ measurement.

The procedure for the rate calculation can be divided into several steps:

- for the single pion production reaction, the phase space density of the three particle final states is calculated numerically using the CERN library routine GENBOD [19]
- the inelastically scattered electrons are tracked through the G0 spectrometer in the G0 Geant simulation program
- the electron momentum range and solid angle are calculated from the Monte Carlo simulation by requiring that the electrons generated in the target track through a particular Cryostat Exit Window Detector segment and particular Focal Plane Detector segment
- beam current, target length and thickness, and luminosity are assumed to be the same as for the elastic scattering experiment [13], and are represented in Table 2.

Average current:	40 μA
Target length:	20 cm
Luminosity:	$2.1 \times 10^{38}\ cm^{-2} s^{-1}$

Table 2: Beam and target parameters for luminosity determination.

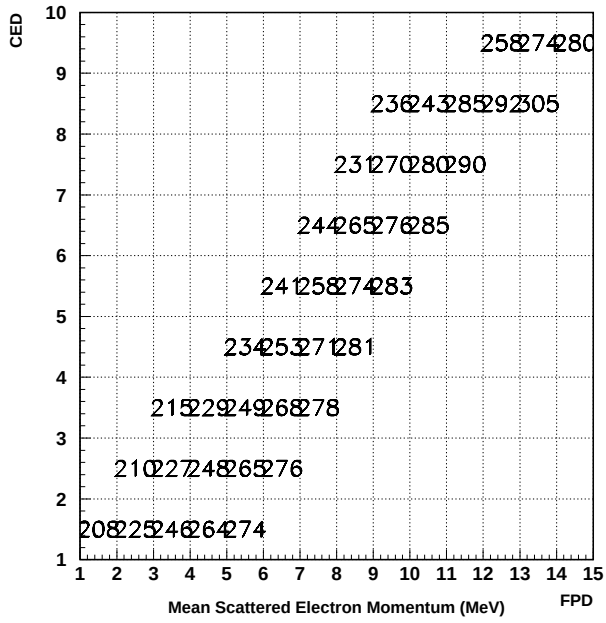

Figure 11: Scattered electron momentum (in MeV) in FPD-CED space for E=0.730 GeV. As an example, the distribution of coincidences between CED number 1 and FPD number 1 has a mean momentum of 208 MeV.

Some results from the procedure described can be seen for a beam energy E=0.730 GeV in Fig.'s 11 and 12, where the scattered electron momentum and angle, respectively, are shown for the Δ resonance in the space of Focal Plane Detector-Cryostat Exit Detector coincidences.

Finally, calculated rates in the FPD-CED space for the same beam energy E=0.730 GeV are shown in Fig. 13.

4 Statistical Uncertainties of the Measured Asymmetries

In the previous two sections, we have described a procedure for calculating inelastically scattered electron kinematics, cross section and counting rates for particular CED segment-FPD segment coincidences. The asymmetry is then determined from yields for the two beam helicities (each measured for a time T_h) as [13]:

$$A^{meas} = \frac{Y_+ - Y_-}{Y_+ + Y_-}, \tag{3}$$

where

$$Y_h = \frac{Rate \times T_h}{Q_h} = \frac{N_h}{Q_h}, \tag{4}$$

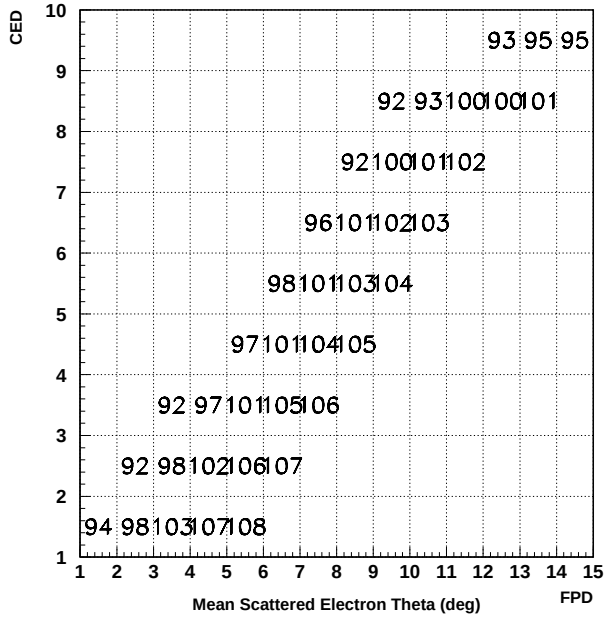

Figure 12: Scattered electron angle (in degrees) in FPD-CED space for E=0.730 GeV.

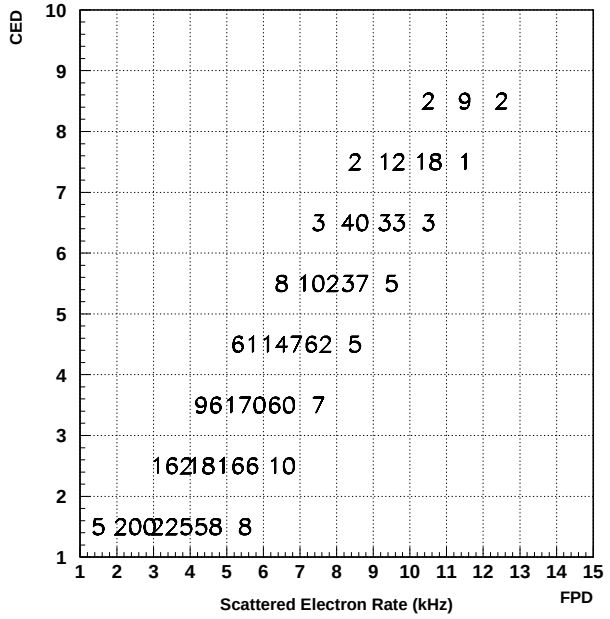

Figure 13: Inelastic electron counting rates (in kHz) in FPD-CED space for E=0.730 GeV.

and N_h and Q_h are the total number of counts in the detectors and the beam charge passing through the target in time T_h, respectively.

The number of counts in the detectors for the two beam helicities is approximately equal, $N_+ \simeq N_- = N/2$, where N is the total number of counts. Neglecting, for now, any dilution factor, the statistical uncertainty we expect to achieve is simply:

$$\Delta A^{meas} = \frac{1}{\sqrt{N}}. \tag{5}$$

While a detailed description of the $N \to \Delta$ transition asymmetry is given in previous sections and the appendices, to calculate the statistical precision of the proposed measurement, we use only the dominant leading term in the asymmetry,

$$A = \frac{G_F}{\sqrt{2}} \frac{Q^2}{2\pi\alpha} \tilde{\alpha}, \tag{6}$$

where Q^2 is the four momentum transfer squared, $G_F = 1.17 \times 10^{-5} (\mathrm{GeV}^{-2})$ is the Fermi coupling constant, $\alpha = 1/137.04$ is the electromagnetic coupling constant, and $\tilde{\alpha}$ is taken to be -0.5536 (with the standard model value of $\sin^2\theta_W = 0.2236$).

The expected statistical uncertainties for inelastic asymmetry measurements made during the same running period as the elastic asymmetry measurements are shown in Fig. 1 for three beam energies. The running time for each measurement is assumed to be 700 hours. To determine the expected statistical accuracy for each Q^2, we have taken the weighted average of the expected uncertainties of all the FPD-CED coincidence bins. The same procedure is performed to obtain the expected statistical accuracy for $G^A_{N\Delta}$ shown in Fig. 2 as a function of Q^2.

5 Background Consideration

In the presence of background, the measured asymmetry A_m is related to the inelastic asymmetry A_i by the following expression [13]:

$$A_m = \frac{A_i R_i + A_b R_b}{R_i + R_b} \tag{7}$$

where R_i and R_b (A_i and A_b) are the total counting rates (asymmetries) for the inelastic and the background events, respectively.

The magnetic analysis of the G0 spectrometer and collimator system ensures that only negatively charged particles scattered from the target will reach both sets of detectors. For extraction of the axial transition form factor $G^A_{N\Delta}(Q^2)$, we have limited our acceptance to the region below where inelastically scattered electrons which have created two pions in the target are detected. There can be, however, π^-'s from the target which can be accepted into this region. These π^-'s originate from two sources: from the $ep \to ep\pi^+\pi^-$ reaction in the hydrogen target, and from single π^- production on the neutrons in the aluminum target end caps.

For measurements on hydrogen, which is the focus of this proposal, we can make estimates of the amount of contamination from π^-'s using the same programs written by Lightbody and O'Connell [16], which we used to estimate the electron rates, as well as MAID2000, a program which calculates pion photo and electroproduction on the nucleon. We found that both programs produce similar rates which are in agreement with the results of π^- cross section measurements

performed in Hall C [20], where both electrons and π^-'s were detected at an angle of $\theta = 135^\circ$ for beam electrons of 824 MeV incident on a LH_2 target.

Our pion rate estimates, an example of which we present in Fig. 14 in CED-FPD space for the $ep \to ep\pi^+\pi^-$ reaction for an incident beam energy of 585 MeV, shows a significant, $\sim 100\%$ π^- contamination which increases up to $\sim 150\%$ for a beam energy of 730 MeV. Fortunately, because the π^-'s and electrons have very different masses, their flight times from the target to each detector can vary substantially. Shown in Fig.'s 15 and 16 are the flight times for both electrons and π^-'s from the target to selected CED's and FPD's for beam energy of 585 MeV. The peak earlier in time corresponds to the electrons, while the peak later in time corresponds to the π^-'s. We now recall the earlier discussion about the backward angle electronics, in which a tight time correlation between a given CED-FPD pair can be made with the beam arrival time at the target. In hardware, a coincidence can be made between these three signals with sufficiently tight time windows to substantially reduce the number of π^-'s which will contribute. Imposing a 3 ns time window around the electron peak in each CED and FPD, corresponding to 8 σ away from the center of the electron peak where the probability of an electron arriving is of order less then 10^{-8}, we obtain the resulting π^- rates as shown in Fig. 17. Thus, this time of flight cut can substantially reduce the number of π^-'s contributing to the asymmetry in the $N \to \Delta$ transition. For this example, the remaining π^-'s constitute only $\sim$ 4-5% contamination fora beam energy of 585 MeV, but still as large as $\sim 70\%$ for a beam energy of 730 MeV. The π^- rate for the lowest beam energy studied (424 MeV) is substantially lower than for a 585 MeV beam, and the resulting π^-'s arrive at each CED or FPD nearly 10 ns later than the electrons. Thus, this procedure effectively eliminates the π^- contribution at this lower beam energy. Including a dilution of the asymmetry from the contribution of π^-'s results in an increase in the error, mainly at the 730 MeV beam energy point where the increase in error on the asymmetry (and on the form factor $G^A_{N\Delta}$) is 8/5, and will result in a somewhat poorer determination of the axial mass ($\delta M_A = 0.062$). This expected result is still $\sim 50\%$ better than the best determination from neutrino experiments.

Although background subtraction using the time of flight technique will be sufficient to perform the experiment proposed here, there is in addition to this another favorable development for our measurement of the $N \to \Delta$ asymmetry. For the quasielastic measurements on deuterium to be proposed at the next PAC, the π^- contamination to both the elastic and inelastic channels is more severe due to single π^- production on the neutrons in deuterium. For those measurements, some particle identification will be required to reject the large number of π^-'s expected from the target, and work is presently underway on the design of a Čerenkov detector to achieve this. Such a detector will completely eliminate pions and bring our measurement precision back to the values from quoted at the beginning of this proposal.

The π^- rate from single π^- production on the neutrons in the aluminum target end caps has also been estimated from the Lightbody/O'Connell code, and was found to be an order of magnitude smaller than the rate from the $ep \to ep\pi^+\pi^-$ reaction, with similar angular and time dependence. Thus, the procedure for reducing this rate in the region of the Δ outlined above will have a similar effect on these π^-'s, even though they constitute a much smaller contamination than the π^-'s from the two pion production mechanism.

Finally, due to the finite length of the LH_2 target, the incident beam electrons can lose energy (radiating bremsstrahlung photons) before scattering from a target proton. There will therefore be an elastic "radiative tail" which will contaminate the inelastic measurement. The yield for the elastic "radiative tail" underneath the Δ resonance can be estimated by knowing

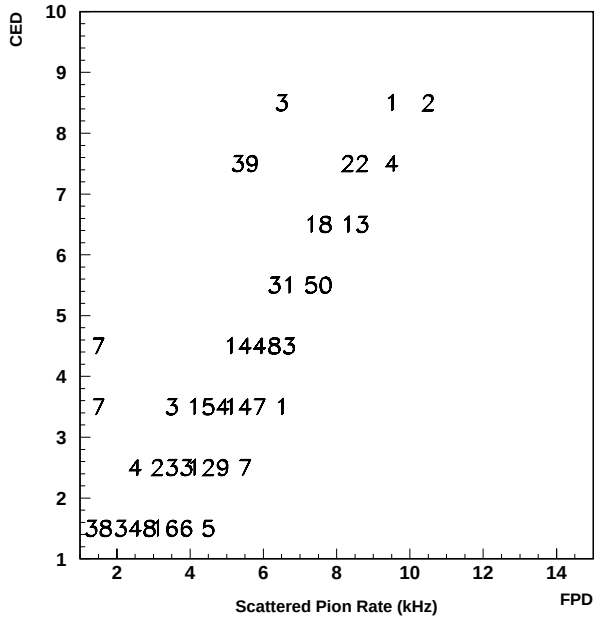

Figure 14: Pion counting rates (in kHz) in FPD-CED space for E=0.585 GeV without time of flight cut.

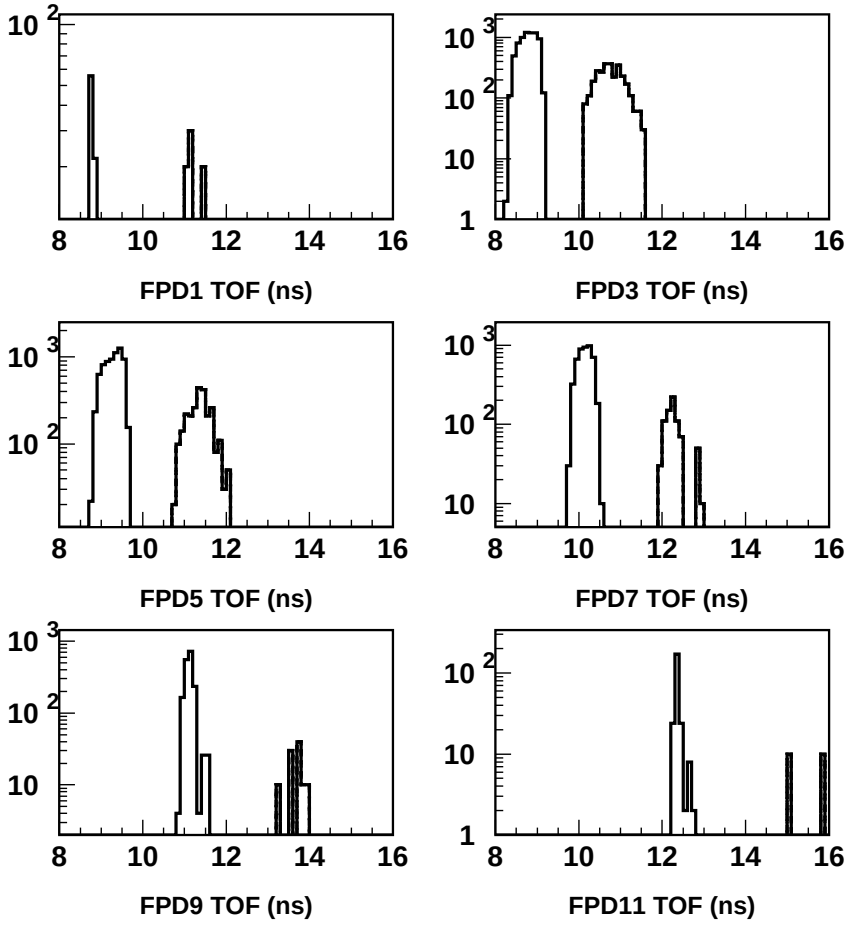

Figure 15: Time of flight separation between electrons and pions at the Focal Plane Detectors for E=0.585 GeV.

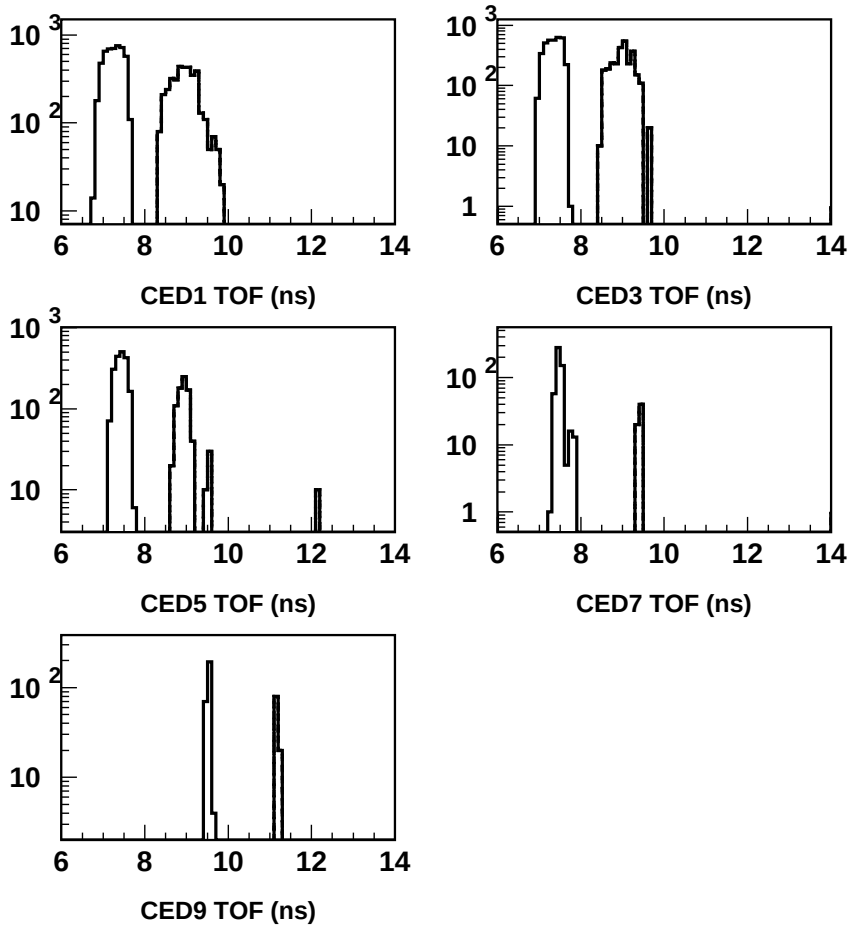

Figure 16: Time of flight separation between electrons and pions at the Cryostat Exit Detectors for E=0.585 GeV.

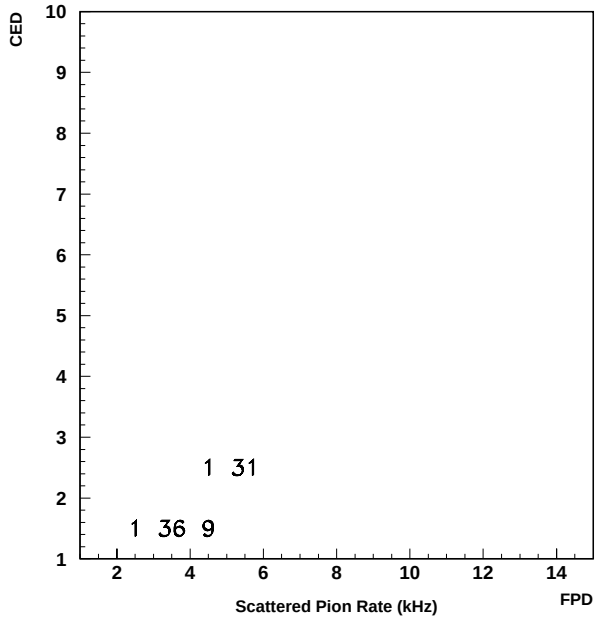

Figure 17: Pion counting rates (in kHz) in FPD-CED space for E=0.585 GeV with the time of flight cut 1.5 ns from the electrons peak position.

how the cross sections for bremsstrahlung and elastic scattering depend on electron and photon energy [21]. Because these measurements will be performed with different beam energies, different amounts of the elastic radiative tail will contribute, depending on which beam energy is used. In the worst case, corresponding to the lowest beam energy, we estimate that the yield from this contamination is of order 1% of the inelastic pion production yield. In addition, the elastic parity violating asymmetry will be measured, allowing us to calculate the contribution to the inelastic asymmetry from this background process. Thus, we conclude that the contribution from the elastic radiative tail to the asymmetry in the inelastic channel is small, and easily correctable.

6 Summary and Requested Beam Time and Support

We are requesting no additional beam time for these measurements, but rather for the parity violating $N \rightarrow \Delta$ measurements to continue to be recognized as an officially approved TJNAF experiment. The measurements described throughout this proposal will be made during the same running period as the G0 experiment in the backward angle mode. In addition, all beam, hardware, and electronics requirements for the G0 backward angle elastic measurements are sufficient to complete the inelastic measurements. Coincidences between the Focal Plane and Cryostat Exit Detectors discussed throughout this proposal are necessary to separate the elastic and threshold inelastic channels during the G0 backward angle measurements, and allow the parity violating asymmetry to be mapped out across the Δ resonance simultaneously. These measurements provide direct access to the axial transition form factor $G^A_{N\Delta}$, the Q^2 dependence of which we will be able to map out in the range $0.1 \leq Q^2 \leq 0.5$ (GeV/c)^2, and represent the first determination of this form factor in the neutral current sector of the weak interaction.

A Formalism

The coupling of electrons to quarks in the nucleon through the exchange of a Z^0 boson can be seen in Fig. 18, where we show the first order Feynman diagram for this exchange between an electron with four momentum K and target nucleon with four momentum P.

The momentum of the scattered electron is K', and the momentum and of the other outgoing particle is P'. The electron couples to the Z^0 boson according to

$$\langle K'|j^Z_\mu|K\rangle \;=\; \bar{u}(K')[g_{V,e}\gamma_\mu + g_{A,e}\gamma_\mu\gamma_5]u(K) \tag{8}$$

showing explicitly the vector-axial vector structure of the weak neutral current interaction. The vector and axial-vector couplings ($g_{V,e}$ and $g_{A,e}$) are functions of standard model parameters, given in Appendix A.

For the Z^0-nucleon coupling, the weak neutral current takes on different forms for the elastic and inelastic channels. In the elastic channel, we have

$$\langle P'|J^Z_\mu|P\rangle \;=\; \bar{u}(P')[\gamma_\mu F_1^Z + i\frac{\sigma_{\mu\nu}q^\nu}{2M}F_2^Z + \gamma_\mu\gamma_5 G_A^Z]u(P) \tag{9}$$

where, again, the vector-axial vector nature of the weak neutral current is evident. The neutral weak vector (F_1^Z,F_2^Z) and axial vector (G_A^Z) form factors of the nucleon (which are functions only of Q^2) can be expressed in terms of the individual quark form factors [22]; it is through these weak neutral form factors that the strange quark content of the nucleon can be accessed.

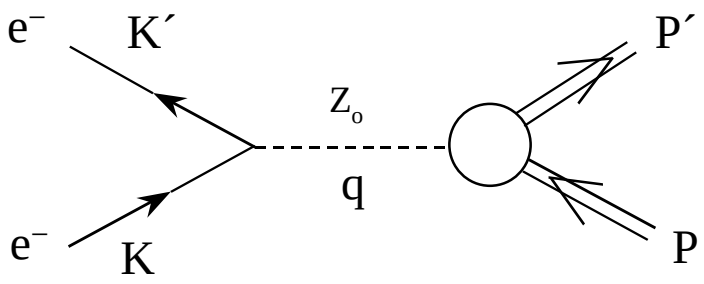

Figure 18: Feynman diagram for Z^0 exchange

In the inelastic Δ channel, the neutral current is somewhat more complicated in its general form [23],

$$\begin{aligned}\langle P'|J^Z_\mu|P\rangle &= \bar{U}^\lambda(P')[(\tfrac{C^Z_{3V}}{M}\gamma^\nu + \tfrac{C^Z_{4V}}{M^2}P'^\nu + \tfrac{C^Z_{5V}}{M^2}P^\nu)(g_{\lambda\mu}g_{\rho\nu} - g_{\lambda\rho}g_{\mu\nu})q^\rho\gamma_5 \; + \; C^Z_{6V}g_{\lambda\mu}\gamma_5 \\ &\quad +(\tfrac{C^Z_{3A}}{M}\gamma^\nu + \tfrac{C^Z_{4A}}{M^2}P'^\nu)(g_{\lambda\mu}g_{\rho\nu} - g_{\lambda\rho}g_{\mu\nu})q^\rho + C^Z_{5A}g_{\lambda\mu} + \tfrac{C^Z_{6A}}{M^2}P_\lambda q_\mu)]u(P) \qquad (10)\end{aligned}$$

but the vector-axial vector nature can still be seen. In this expression, $U^\lambda(P')$ is the Rarita-Schwinger field describing the spin-$\frac{3}{2}$ Δ resonance [24], P and P' are, respectively, the momenta of the nucleon and the Δ, and $q \; = \; P' - P$.

The weak transition form factors in Eq. (3), which are functions only of Q^2, can be related to the electroproduction and weak charged current production of the Δ by performing a rotation in isospin space and exploiting the conserved vector current (CVC) hypothesis [23]. In the notation of Llewellyn-Smith [25], they become

$$\begin{aligned} C^Z_{iV} &= \alpha C^\gamma_i, \quad i = 3,4,5 \; , \\ C^Z_{6V} &= 0 \; , \\ C^Z_{iA} &= -\beta C^A_i, \quad i = 3,4,5,6 \; , \end{aligned} \qquad (11)$$

where α and β are the quark-Z^0 couplings (given in Appendix A). The electroproduction form factors are denoted by C^γ_i, and the C^A_i are $-\frac{1}{\sqrt{3}}$ times the charged-current axial vector weak transition form factors.

To make the isospin structure of this transition evident, it is useful to examine the parity violating phenomenological Lagrangian for electron nucleon scattering [26],

$$\begin{aligned} L \; = \; & -\tfrac{G_F}{2}\{\bar{e}\gamma_\lambda\gamma_5 e[\tfrac{\tilde{\alpha}}{2}(\bar{u}\gamma_\lambda u - \bar{d}\gamma_\lambda d) + \tfrac{\tilde{\gamma}}{2}(\bar{u}\gamma_\lambda u + \bar{d}\gamma_\lambda d)] \\ & +\bar{e}\gamma_\lambda e[\tfrac{\tilde{\beta}}{2}(\bar{u}\gamma_\lambda\gamma_5 u - \bar{d}\gamma_\lambda\gamma_5 d) + \tfrac{\tilde{\delta}}{2}(\bar{u}\gamma_\lambda\gamma_5 u + \bar{d}\gamma_\lambda\gamma_5 d) + ...]\}, \end{aligned} \qquad (12)$$

where $(\bar{e}, e)$, $(\bar{u}, u)$, and $(\bar{d}, d)$ represent Dirac spinors for the electrons and quarks, the electron-quark coupling constants have the following meaning:

$\tilde{\alpha}$: isovector axial vector electron – vector quark,

$\tilde{\beta}$: isovector vector electron – axial vector quark,

$\tilde{\gamma}$: isoscalar axial vector electron – vector quark,

$\tilde{\delta}$: isoscalar vector electron – axial vector quark,

with standard model relations

$$\tilde{\alpha} \; = \; -(1 - 2\sin^2\theta_W)$$

$$\tilde{\beta} \; = \; -(1 - 4\sin^2\theta_W)$$

$$\tilde{\gamma} \; = \; \frac{2}{3}\sin^2\theta_W$$

$$\tilde{\delta} \; = \; 0.$$

The dots in Eq. (5) denote isoscalar axial heavy quark (s,c,...) currents.

Because the $N \to \Delta$ transition is purely isovector, the parity violating asymmetry for Δ production takes the form [27]

$$A_{RL} \;=\; \frac{d\sigma_R - d\sigma_L}{d\sigma_R + d\sigma_L} \;=\; \frac{G_F}{\sqrt{2}}\frac{Q^2}{2\pi\alpha}[\tilde{\alpha} + \tilde{\beta}F(Q^2, E, E', \theta_e)], \tag{13}$$

where $d\sigma_{R(L)} \equiv \frac{d^2\sigma}{dq^2 dW^2}|_{R(L)}$ is the differential cross section for scattering electrons of positive (negative) helicity from the nucleon, $Q^2 = -(K - K')^2$, $W^2 = (P + K - K')^2$, α in this case is the electromagnetic coupling constant, and $F(Q^2, E, E', \theta_e)$ contains all of the weak transition form factors discussed above, in addition to dependence on kinematic variables. Specifically, we write (see Appendix A),

$$F(Q^2, E, E', \theta_e) \;=\; \frac{(E + E')}{M} H^{EM}(Q^2, \theta_e) G^A_{N\Delta}(Q^2), \tag{14}$$

where $H^{EM}(Q^2, \theta_e)$ contains the electromagnetic form factors $C_i^\gamma(Q^2)$ $(i = 3, 4)$ (which will be more precisely determined in future Hall B experiments), and $G^A_{N\Delta}(Q^2)$ contains the axial transition form factors $C_i^A(Q^2)$ $(i = 3, 4, 5, 6)$. Thus, for a pure isovector $N \to \Delta$ transition, the parity violating asymmetry consists of two terms: the axial vector electron-vector quark coupling, which is given explicitly by the electron-quark coupling constant $\tilde{\alpha}$, and the vector electron-axial vector quark coupling, which contains the axial vector transition form factor $G^A_{N\Delta}$. The relative strengths of these two terms is determined by the coupling constants $\tilde{\alpha}$ and $\tilde{\beta}$, which, with the standard model value of $\sin^2\theta_W$=0.2236, take on the numerical values

$$\tilde{\alpha} \;=\; -0.5536 \;\;,\;\; \tilde{\beta} \;=\; -0.1056.$$

Thus, for reasonable $F(Q^2, E, E', \theta_e)$ values, the leading $\tilde{\alpha}$ term contributes roughly 75% to this parity violating asymmetry. Using estimates for the $N \to \Delta$ weak transition form factors, $F(Q^2, E, E', \theta_e)$ is found to be of order unity in this kinematic regime [27], in contrast to the high energy limit ($\frac{Q^2}{2ME} \ll 1$), where $F(Q^2, E, E', \theta_e) \ll 1$ [28]. Consequently, using relatively low beam energies and detecting electrons scattered at backward angles will enhance our sensitivity to the $N \to \Delta$ axial transition form factor $G^A_{N\Delta}(Q^2)$.

This form factor can be accessed in a number of different ways, and is usually parameterized in terms of the axial-vector mass M_A, according to the Adler model [12], in which a modified dipole form is used. In neutrino induced weak Δ^{++} production, $G^A_{N\Delta}(Q^2)$ can be determined through the Q^2 dependence of the differential cross section for this reaction, and therefore represents a determination of this form factor in the charged current sector of the weak interaction. An early study of neutrino induced weak Δ^{++} production from the proton [29] yielded a value of $M_A = 0.95 \pm 0.09$. A more recent study [30] of this reaction on deuterium between $0.1 \leq Q^2 \leq 3.0$ (GeV/c)^2 yielded $M_A = 1.28^{+0.08}_{-0.10}$, but this value showed sensitivities to deuteron structure and cuts on spectator nucleon momentum. The measurements described in this proposal will provide the first determination of M_A in the neutral current sector. Comparison between these two types of measurements of the same physical quantity can therefore provide us with an indication of how important isospin breaking corrections are in the weak interaction [31]. In $\pi^-\Delta^{++}$ electroproduction, coincidence differential cross section measurements are typically performed near threshold [32, 33, 34], in which the scattered e^- and the electroproduced π^- are detected. To interpret these data, low energy theorems are extrapolated from threshold through

the resonance region, and use is made of the partially conserved axial vector current (PCAC) hypothesis. To date, data from experiments of this type have instead been interpreted, using the theoretical results of Adler and Weisberger [35], in terms of the nucleon axial vector form factor $G_A(Q^2)$. The TJNAF PAC approved E94-005 experiment [32], however, will use the above mentioned techniques and approximations to extract $G^A_{N\Delta}$ for larger Q^2 values than considered in this proposal ($0.5 \leq Q^2 \leq 2.5$ (GeV/c)^2). In contrast, the measurement of the parity violating asymmetry in the $N \rightarrow \Delta$ transition proposed here gives direct access to $G^A_{N\Delta}(Q^2)$, without PCAC or extrapolation of low energy theorems. Because PCAC, which essentially states that all of the axial current is carried away by the electroproduced π^-, is expected to be broken at the 5-7% level [31], comparison of the determination of $G^A_{N\Delta}(Q^2)$ from the electroproduction experiments with the determination through the parity violating asymmetry in the $N \rightarrow \Delta$ transition can provide some insight into PCAC violation.

Although these asymmetry measurements give us direct access to $G^A_{N\Delta}(Q^2)$, a correct determination of this form factor can only be done if the non-resonant contributions to the asymmetry are small, or understood. With an extensive data base of single pion photoproduction cross section measurements in the region of the Δ [36, 37, 38, 39, 40, 41], a model independent determination of the resonant and non-resonant contributions to this process has been made [42], allowing for a determination of the $E2/M1$ ratio for the resonance, free from uncertainties associated with theoretical models of background contributions. This ratio, recognized early on as a crucial quantity to test theories of effective forces between quarks needed to understand hadron structure [43], could be extracted with no model dependence, allowing for a cleaner interpretation of the data and their implications for theoretical models. While it is true that the allowed phase space for inclusive single π electroproduction from the proton has its dominant contribution from the resonant Δ^+, there are contributions from non-resonant processes which must be understood for a proper interpretation of the data (see Appendix C). To understand these contributions to the asymmetry, a similar model independent determination of the resonant and non-resonant pieces must be performed throughout the entire Q^2 range studied. Several measurements planned for Hall B [9] will address this issue directly by mapping out the Q^2 dependence of both resonant and non-resonant multipoles in single π electroproduction for $Q^2 \leq 4$ (GeV/c)^2. Although these experiments focus on determining the electromagnetic ratio $\frac{E_{1+}}{M_{1+}}$ to high precision (errors of order 0.005), the combination of angular distributions and polarization observables will allow for determinations of all of the s and p wave multipoles, along with their isospin decomposition, to somewhat less precision (errors of order 0.04) [9].

Until such electroproduction data exist to constrain the non-resonant multipoles, we must rely on models for an estimate of what contribution the non-resonant background will make to the parity violating asymmetry in the $N \rightarrow \Delta$ transition. One such estimate can be made by comparing two calculations of this asymmetry: one for pure Δ production [23], and one for single π production at the same energy [44], which includes contributions from all Born diagrams and ρ and ω meson contributions in addition to the Δ. These two calculations are within 10% of each other in the Q^2 range considered in this proposal, suggesting that the contribution to the asymmetry from the non-resonant background is indeed small in this kinematic regime. More recently, a phenomenological model with effective Lagrangians [11] was used to calculate the parity violating asymmetry in π electroproduction from the proton in the energy region between pion threshold through the Δ resonance. In these results, contributions from the resonant, non-resonant, and interference terms are given separately as a function of both Q^2 and k_γ (photon equivalent energy), providing a useful guide for understanding the sensitivity of the asymmetry

to these separate contributions in varying kinematic regimes. In Fig. 1 we show the calculations of Ref. [11] near the peak of the Δ resonance for these different contributions to the asymmetry at an incident beam energy of 0.8 GeV, normalized to the Q^2 of the reaction, as a function of Q^2, along with our expected statistical uncertainty for the inelastic $\vec{e}+p$ measurements to be made concurrent with the G0 elastic $\vec{e}+p$ measurements. As in the previous estimate based on the calculations of Ref.'s [23] and [44], the full calculation and the resonant contribution differ by at most 10% in this same Q^2 regime, giving us confidence that a meaningful interpretation of these data is possible. With the non-resonant contributions sufficiently constrained, we can make an estimate of what precision we can achieve on the axial transition form factor $G^A_{N\Delta}$, which we plot in Fig. 2, using the modified dipole parameterization of Adler [12]. From the expected statistical precision, we can extract the axial mass M_A from $G^A_{N\Delta}$ with an absolute error of 0.045, roughly a factor of 2 better than any of the neutrino experiments which have extracted this parameter.

B Details of the Asymmetry

In this appendix, we relate the notation used here to notations used by other authors [26, 23], and show the explicit kinematic dependences of the coefficients of the electromagnetic and weak transition form factors.

In the notation of Ref. [23], the asymmetry, containing only resonant terms, is written

$$A_{RL} = -\frac{2Q^2}{e^2(Q^2+M_Z^2)}\{\alpha g_{A,e} + \beta g_{V,e}\frac{2(E+E')}{M}\frac{W_3\sin^2\frac{\theta_e}{2}}{2W_1^{EM}\sin^2\frac{\theta_e}{2}+W_2^{EM}\cos^2\frac{\theta_e}{2}}\}, \qquad (15)$$

where $g_{V,e}$ and $g_{A,e}$, are given, in the minimal $\mathrm{SU}(2)_L\times\mathrm{U}(1)$ model, by [23]

$$g_{V,e} = \frac{-e}{4\sin\theta_W\cos\theta_W}(1-4\sin^2\theta_W)$$

and

$$g_{A,e} = \frac{e}{4\sin\theta_W\cos\theta_W},$$

where e is the electron charge, and $\sin^2\theta_W$ is the weak mixing angle, α and β are given by [23]

$$\alpha = \frac{e}{2\sin\theta_W\cos\theta_W}(1-2\sin^2\theta_W),$$

$$\beta = -\frac{e}{2\sin\theta_w\cos\theta_W},$$

the structure functions are given by [23]

$$\begin{aligned}
W_1^{EM} &= \frac{c}{6M^4}\{a^2[D_3(Q^2)]^2 + b^2[D_4(Q^2)]^2 + abD_3(Q^2)D_4(Q^2)\},\\
W_2^{EM} &= \frac{2Q^2}{3M^2}\{a[D_3(Q^2)]^2 + c[D_4(Q^2)]^2 + bD_3(Q^2)D_4(Q^2)\}, \qquad (16)\\
W_3 &= \frac{1}{3M^2}[2aD_3(Q^2)+bD_4(Q^2)]\{(b-2c)\frac{M}{2M'}C_3^A(Q^2)+\frac{b}{2}C_4^A(Q^2)-M^2C_5^A(Q^2)\},
\end{aligned}$$

with

$$\begin{aligned} a &= (M+M')^2+Q^2, \\ b &= (M+M')(M-M')+Q^2, \\ c &= (M-M')^2+Q^2, \end{aligned} \tag{17}$$

and

$$\begin{aligned} D_3(Q^2) &= -\frac{M}{M'}C_3^\gamma(Q^2), \\ D_4(Q^2) &= \frac{M}{M'}C_3^\gamma(Q^2)+C_4^\gamma(Q^2). \end{aligned} \tag{18}$$

To convert coupling strengths, consider only the first term, and assume $Q^2 \ll M_Z^2$. Then,

$$\begin{aligned} A_{RL} &= -\frac{2Q^2}{e^2M_Z^2}\alpha g_{A,e} \\ &= -\frac{2Q^2}{e^2M_Z^2}\left(\frac{e}{2\sin\theta_W\cos\theta_W}\right)\left(\frac{e}{4\sin\theta_W\cos\theta_W}\right)(1-2\sin^2\theta_W) \\ &= \frac{2Q^2}{M_Z^2}\frac{1}{8\sin^2\theta_W\cos^2\theta_W}[-(1-2\sin^2\theta_W)]. \end{aligned}$$

Now, we use [26]

$$M_W^2 = M_Z^2\cos^2\theta_W,$$

to get

$$A_{RL} = \frac{2Q^2}{8M_W^2\sin^2\theta_W}[-(1-2\sin^2\theta_W)].$$

Next, we use [26]

$$\frac{G_F}{\sqrt{2}} = \frac{g^2}{8M_W^2}$$

and

$$e = g\sin\theta_W$$

to obtain

$$A_{RL} = \frac{2Q^2}{e^2}\frac{G_F}{\sqrt{2}}[-(1-2\sin^2\theta_W)].$$

Finally, we use

$$e^2 = 4\pi\alpha$$

to get

$$\begin{aligned} A_{RL} &= \frac{G_F}{\sqrt{2}}\frac{Q^2}{2\pi\alpha}[-(1-2\sin^2\theta_W)] \\ &= \frac{G_F}{\sqrt{2}}\frac{Q^2}{2\pi\alpha}\tilde{\alpha}. \end{aligned}$$

Similarly,

$$-\frac{2Q^2}{e^2M_Z^2}\beta g_{V,e} = \frac{G_F}{\sqrt{2}}\frac{Q^2}{2\pi\alpha}\tilde{\beta}.$$

We now have

$$A_{RL} = \frac{G_F}{\sqrt{2}}\frac{Q^2}{2\pi\alpha}\{\tilde{\alpha}+\tilde{\beta}\frac{(2\tan^2\frac{\theta_e}{2})W_3}{(2\tan^2\frac{\theta_e}{2})W_1^{EM}+W_2^{EM}}\}, \tag{19}$$

where W_1^{EM}, W_2^{EM}, and W_3 are given by Eq. (16) above, and we have divided both numerator and denominator of Eq. (15) by $\cos^2\frac{\theta_e}{2}$ (we note that no measurements will be made at θ_e=180°). Carrying through some algebra yields

$$\begin{aligned} (2\tan^2\frac{\theta_e}{2})W_1^{EM}+W_2^{EM} = {} & h_{33}(Q^2,\theta_e)[C_3^\gamma(Q^2)]^2+h_{34}(Q^2,\theta_e)C_3^\gamma(Q^2)C_4^\gamma(Q^2) \\ & +h_{44}(Q^2,\theta_e)[C_4^\gamma(Q^2)]^2, \end{aligned} \tag{20}$$

where

$$\begin{aligned} h_{33}(Q^2,\theta_e) &= \frac{1}{3M'^2}[(a^2+b^2-ab)c\frac{\tan^2\frac{\theta_e}{2}}{M^2}+2(a+c-b)Q^2], \\ h_{34}(Q^2,\theta_e) &= \frac{1}{3MM'}[(2b^2-ab)c\frac{\tan^2\frac{\theta_e}{2}}{M^2}+2(2c-b)Q^2], \\ h_{44}(Q^2,\theta_e) &= \frac{1}{3M^2}[b^2c\frac{\tan^2\frac{\theta_e}{2}}{M^2}+2cQ^2], \end{aligned} \tag{21}$$

with a, b, and c defined in Eq. (17).

Similarly,

$$\begin{aligned} (2\tan^2\frac{\theta_e}{2})W_3 = {} & [h_3(Q^2,\theta_e)C_3^\gamma(Q^2)+h_4(Q^2,\theta_e)C_4^\gamma(Q^2)]\times \\ & [g_3(Q^2)C_3^A(Q^2)+g_4(Q^2)C_4^A(Q^2)+g_5(Q^2)C_5^A(Q^2)], \end{aligned} \tag{22}$$

where

$$\begin{aligned} h_3(Q^2,\theta_e) &= \frac{2M}{3M'}(b-2a)\frac{\tan^2\frac{\theta_e}{2}}{M^2}, \\ h_4(Q^2,\theta_e) &= \frac{2}{3}b\frac{\tan^2\frac{\theta_e}{2}}{M^2}, \\ g_3(Q^2) &= \frac{M}{2M'}(b-2c), \\ g_4(Q^2) &= \frac{b}{2}, \\ g_5(Q^2) &= -M^2. \end{aligned} \tag{23}$$

Substituting Eq.'s (20) and (22) into Eq. (19) yields

$$A_{RL} = \frac{G_F}{\sqrt{2}}\frac{Q^2}{2\pi\alpha}[\tilde{\alpha} + \tilde{\beta}F(Q^2, E, E', \theta_e)], \tag{24}$$

where

$$F(Q^2, E, E', \theta_e) = \frac{(E+E')}{M}H^{EM}(Q^2, \theta_e)G^A_{N\Delta}(Q^2), \tag{25}$$

with

$$H^{EM}(Q^2, \theta_e) = \frac{h_3(Q^2, \theta_e)C_3^\gamma(Q^2) + h_4(Q^2, \theta_e)C_4^\gamma(Q^2)}{h_{33}(Q^2, \theta_e)[C_3^\gamma(Q^2)]^2 + h_{34}(Q^2, \theta_e)C_3^\gamma(Q^2)C_4^\gamma(Q^2) + h_{44}(Q^2, \theta_e)[C_4^\gamma(Q^2)]^2}, \tag{26}$$

and

$$G^A_{N\Delta}(Q^2) = g_3(Q^2)C_3^A(Q^2) + g_4(Q^2)C_4^A(Q^2) + g_5(Q^2)C_5^A(Q^2). \tag{27}$$

We note here that, in full generality, $C_6^A(Q^2)$ would contribute (see Eq. (3)), but enters into this part of the asymmetry with a factor of $\frac{m_e}{M}$ and is therefore neglected [23]. Additionally, the form of $H^{EM}(Q^2, \theta_i)$ depends on the assumption that $C_5^\gamma(Q^2) = 0$. The physics justification for this assumption is two-fold: a) the theory of the spin-$\frac{3}{2}$ field requires that $C_4^\gamma(Q^2) = C_5^\gamma(Q^2) = 0$, and b) the single pion photoproduction and electroproduction data can be adequately described with $C_4^\gamma(Q^2) = C_5^\gamma(Q^2) = 0$, or $C_5^\gamma(Q^2) = 0$ and $C_4^\gamma(Q^2) = -\frac{M}{M+M'}C_3^\gamma(Q^2)$ [23].

C Discussion of Non-Resonant Background

As discussed throughout this proposal, the yield for single pion electroproduction from the proton is dominated by the $N \to \Delta$ resonance, but there are non-resonant processes which contribute. While estimates have been given as to the contribution these processes make to the parity violating asymmetry, the non-resonant background must be understood for a proper interpretation of the data to be obtained from these proposed measurements. To bring out the main features of the parity violating asymmetry in inclusive π electroproduction in the Δ resonance region, an analysis of the asymmetry obtained from the incoherent summation of the coincident $p\pi^0$ and $n\pi^+$ charge states (*i.e.,* the decay of the Δ^+) has been performed [45]. They find

$$A^\pi_{RL} = -\frac{1}{2}\frac{G_F}{\sqrt{2}}\frac{Q^2}{2\pi\alpha}(\Delta^\pi_{(1)} + \Delta^\pi_{(2)} + \Delta^\pi_{(3)}), \tag{28}$$

where $\Delta^\pi_{(1)}$ corresponds to the axial vector electron-vector quark isovector resonant contribution, $\Delta^\pi_{(2)}$ gives the axial vector electron-vector quark non-resonant background contributions (both isovector and isoscalar), and $\Delta^\pi_{(3)}$ gives the vector electron-axial vector quark contribution (both resonant isovector and non-resonant isoscalar). These terms are given explicitly by

$$\begin{aligned}
\Delta^\pi_{(1)} &= g_A^e\xi_V^{T=1} \\
F^2\Delta^\pi_{(2)} &= -2g_A^e\xi_V^n\sum_l \Re \\
&\times \{v_T[l(l+1)^2(\frac{3}{\sqrt{2}}M^{0*}_{l+}M^{\frac{1}{2}}_{l+} - 3|M^0_{l+}|^2) + l^2(l+1)(\frac{3}{\sqrt{2}}M^{0*}_{l-}M^{\frac{1}{2}}_{l-} - 3|M^0_{l-}|^2)
\end{aligned}$$

$$
\begin{aligned}
&+ \quad (l+2)(l+1)^2(\frac{3}{\sqrt{2}}E^{0*}_{l+}E^{\frac{1}{2}}_{l+} - 3|E^0_{l+}|^2) + l^2(l-1)(\frac{3}{\sqrt{2}}E^{0*}_{l-}E^{\frac{1}{2}}_{l-} - 3|E^0_{l-}|^2)] \\
&+ \quad v_L[(l+1)^3\frac{3}{\sqrt{2}}S^{0*}_{l+}S^{\frac{1}{2}}_{l+} - 3|S^0_{l+}|^2) + l^3(\frac{3}{\sqrt{2}}S^{0*}_{l-}S^{\frac{1}{2}}_{l-} - 3|S^0_{l-}|^2)]\} \qquad (29) \\
F^2\Delta^\pi_{(3)} &= 2g^e_V v_{T'} \sum_l \Re\{l(l+1)^2\tilde{E}^{5*}_{l+}M_{l+} - (l+1)^2(l+2)\tilde{M}^{5*}_{l+}E_{l+} \\
&- \quad l^2(l+1)\tilde{E}^{5*}_{l-}M_{l-} + l^2(l-1)\tilde{M}^{5*}_{l-}E_{l-}\},
\end{aligned}
$$

where the E's, M's, and S's are transverse electric, transverse magnetic, and longitudinal multipoles, respectively [12, 46, 47], their subscripts denote the angular momentum and parity, their superscripts indicate the isospin decomposition,

$$
\begin{aligned}
v_T &= \frac{1}{2}|\frac{Q^2}{q^2}| + \tan^2\frac{\theta_e}{2} \\
v'_T &= \tan\frac{\theta_e}{2}\sqrt{|\frac{Q^2}{q^2}| + \tan^2\frac{\theta_e}{2}} \qquad (30) \\
v_L &= |\frac{Q^2}{q^2}|^2,
\end{aligned}
$$

and F^2 corresponds to the inclusive electromagnetic cross section, normalized to the Mott cross section (in the notation used here, F^2 corresponds to $2W_1^{EM}\sin^2\frac{\theta_e}{2} + W_2^{EM}\cos^2\frac{\theta_e}{2}$). The conversion of coupling constants has been given in Ref. [45], where they find

$$
\begin{aligned}
g^e_A\xi^{T=1}_V &= -2\tilde{\alpha}, \\
-2g^e_A\xi^n_V &= -2(\tilde{\alpha} - 3\tilde{\gamma}).
\end{aligned}
$$

Also, we note that the axial contribution, $F^2\Delta^\pi_{(3)}$, has no isospin decomposition given here. The contributions to this term, however, come from three sources [31]: the dominant isovector piece, which includes the axial transition form factor $G^A_{N\Delta}(Q^2)$; the primordial weak isoscalar axial current, which vanishes in the minimal $\mathrm{SU}(2)_L\times\mathrm{U}(1)$ standard model (and becomes nonvanishing only when weak radiative corrections are included); and the heavy quark isoscalar axial currents, which were originally neglected in writing down the phenomenological Lagrangian for electron nucleon scattering (denoted by dots in Eq. (5)), and are expected to be only a few percent of the isovector contribution [31]. Thus, for a first generation inelastic channel parity violation measurement, the axial term may be taken to have a contribution only from the isovector piece containing the axial transition form factor $G^A_{N\Delta}(Q^2)$. Thus, we may write

$$
A^\pi_{RL} = \frac{G_F}{\sqrt{2}}\frac{Q^2}{q\pi\alpha}[\tilde{\alpha} + (\tilde{\alpha} - 3\tilde{\gamma})\Delta^{\pi'}_{(2)} + \tilde{\beta}F(Q^2, E, E', \theta_e)], \qquad (31)
$$

where $F(Q^2, E, E', \theta_e)$ is given by Eq. (7) and in Appendix A, and

$$
\Delta^{\pi'}_{(2)} = \frac{\Delta^\pi_{(2)}}{-2(\tilde{\alpha} - 3\tilde{\gamma})}. \qquad (32)
$$

As can be seen from Eq. (29), there are an infinite number of multipoles which comprise the non-resonant background contribution to the 1 pion electroproduction asymmetry, with both

isovector and isoscalar pieces. Thus, even in keeping only the leading order multipoles implies that an isospin decomposition is necessary to describe the non-resonant contribution. As discussed earlier, an extensive data base for photoproduction from both the proton and neutron [36, 37, 38, 39, 40, 41] exist, and complete multipole and isospin decompositions have been done at the photon point [48, 42]. Such a decomposition does not exist for finite Q^2, as electroproduction data on neutron targets is quite limited. Once these data exist [9], a more thorough description of the background will be possible.

In addition, this analysis [45] was performed on the incoherent summation of final charge states, where no interference between resonant and non-resonant multipoles contributes. The parity violating asymmetry from inclusive 1 pion electroproduction will certainly have contributions from these interferences, and must be taken into account for a description of these measurements. Again, an estimate of the contributions from both the background and the interferences can be made with the use of a model [11], throughout the entire 1 pion production region. Near the resonance, both of these contributions are expected to be small (see Fig. 1), and contribute with opposite signs, resulting in the resonant contribution dominating the asymmetry. As one moves away from the resonance, the relative sizes of these contributions is expected to change, as can be seen in Fig. 19, where we plot the individual contributions to the asymmetry as a function of photon equivalent energy k_γ, where

$$k_\gamma \;=\; \frac{(E-E')}{2} + \frac{Q^2}{2M}, \tag{33}$$

for two different values of Q^2, along with an estimate of our expected statistical precision to be achieved at each Q^2 value studied in Ref. [11]. At low Q^2, and near threshold, the non-resonant background makes a large contribution, but decreases in strength with increasing excitation energy, while the resonant contribution increases. In the context of this phenomenological model, there is a curious cancellation of non-resonant and interference terms as the excitation energy increases, which persists as a function of Q^2, resulting in a parity violating asymmetry which has very little dependence on excitation energy.

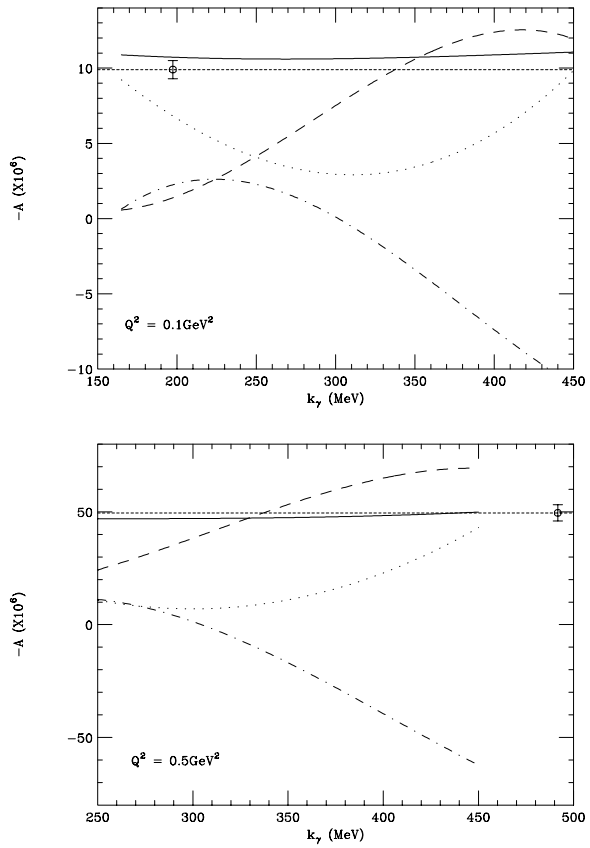

Figure 19: Asymmetries as a function of photon equivalent energy, k_γ, for Q^2=0.1 (GeV/c)^2 (upper) and Q^2=0.5 (GeV/c)^2 (lower), including expected statistical precision for each Q^2 value. The meaning of the curves is the same as in Fig. 1.

References

[1] Nimai C. Mukhopadhyay *et al.,* Nucl. Phys. **A633,** 481 (1998).

[2] M.P. Rekalo, J. Arvieux, E. Tomasi-Gustafsson, nucl-th/0009054 (2000).

[3] L. Alvarez-Ruso, S.K. Singh, M.J. Vicente Vacas, Phys. Rev. **C59,** 3386 (1998).

[4] L. Alvarez-Ruso, E. Oset, S.K. Singh, M.J. Vicente-Vacas, Nucl. Phys. **A663,** 837 (2000).

[5] M.D. Slaughter, hep-ph/9903208.

[6] L. Elouadrhiri, Few Body Syst. Suppl. 11:130-133, 1999.

[7] H. Schmieden, Eur. Phys. J. **A1:** 427 (1998).

[8] T. Sato and T.-S.H. Lee, nucl-th/0010025 (2000).

[9] V. Burkert in N^* *WORKSHOP* - "Partial Wave Analysis," CEBAF, Nov. 9-12, 1995.

[10] R. Hasty et al., SAMPLE collaboration, Science, 15 December 2000.

[11] H.-W. Hammer and D. Drechsel, Z. Phys. **A353**, 321 (1995).

[12] S.L. Adler, Ann. Phys. **50**, 189 (1968).

[13] G0 Technical Design Report, Nuclear Physics Laboratory, University of Illinois at Urbana-Champaign, 1993.

[14] S.P. Wells, LATECH-CAPS-99-03b, G0-99-008, (1999).

[15] C. Murphy, S.P. Wells, and N. Simicevic, LATECH-CAPS-99-11a, G0-99-051, (1999).

[16] J. W. Lightbody and J. S. O'Connel, Computers in Physics **2**, 57 (1988).

[17] F. W. Brasse *et al.,* Nucl. Phys. B **110**, 413 (1976).

[18] F. W. Brasse *et al.,* NC **55A**, 679 (1967).

[19] F. James and M. Roos, CERN computer center program, (1977).

[20] M. Pitt and J. Roche, private communication.

[21] S.M. Seltzer and M.J. Berger, Nucl. Instr. and Meth. B **12**, 95 (1985).

[22] D.H. Beck, Phys. Rev. D **39**, 3248 (1989).

[23] L.M. Nath, K. Schilcher, and M. Kretzschmar, Phys. Rev. D **25**, 2300, 1982.

[24] W. Rarita and J. Schwinger, Phys. Rev. **60**, 61 (1941).

[25] C.H. Llewellyn Smith, Phys. Rep. **3**, 261 (1972).

[26] P.Q. Hung and J.J. Sakurai, Ann. Rev. Nucl. Part. Sci. **31**, 375 (1981).

[27] D.R.T. Jones and S.T. Petcov, Phys. Lett. B **91**, 137 (1980).

[28] R.N. Cahn and F.J. Gilman, Phys. Rev. D **17**, 1313 (1978)

[29] S.J. Barish *et al.,* Phys. Rev. D **19**, 2521 (1979).

[30] T. Kitagaki *et al.,* Phys. Rev. D **42**, 1331 (1990).

[31] T.W. Donnelly, private communication.

[32] L. Elouadrhiri, CEBAF Experiment E94-005.

[33] P. Joos *et al.,* Phys. Lett. B **62**, 230 (1976).

[34] S. Choi *et al.,* Phys. Rev. Lett. **71**, 3927 (1993).

[35] S.L. Adler and W.I. Weisberger, Phys. Rev. **169**, 1392 (1968).

[36] W. Pfeil and D. Schwela, Nucl. Phys. B **45**, 379 (1971).

[37] F.A. Berends and A. Donnachie, Nucl. Phys. B **84**, 342 (1975).

[38] S. Suzuki, S. Kurokawa, and K. Kondo, Nucl. Phys. B **68**, 413 (1974).

[39] I.I. Miroshnichenko *et al.,* Sov. J. Nucl. Phys. **32**, 339 (1980).

[40] V.A. Get'man *et al.,* Sov. J. Nucl. Phys. **38**, 230 (1983).

[41] V.F. Grushin *et al.,* Sov. J. Nucl. Phys. **38**, 881 (1983).

[42] R.M. Davidson and Nimai C. Mukhopadhyay, Phys. Rev. D **42**, 20 (1990).

[43] R.M. Davidson, Nimai C. Mukhopadhyay, and R. Wittman, Phys. Rev. Lett. **56**, 804 (1986).

[44] Sai-Ping Li, E.M. Henley, and W-Y.P. Hwang, Ann. of Phys. **143**, 372 (1982).

[45] M.J. Musolf, T.W. Donnelly, J. Dubach, S.J. Pollock, S. Kowalski, and E.J. Beise, Phys. Rep. **239**, 1 (1994).

[46] S.J. Pollock, Ph.D. Thesis, Stanford University (1987) unpublished.

[47] A.S. Raskin and T.W. Donnelly, Ann. Phys. **191**, 78 (1989).

[48] W.J. Metcalf and R.L. Walker, Nucl. Phys. B **76**, 253 (1974).